Mechanics of *Drosophila* embryogenesis and heat-shock-induced developmental defects

By

Sarah Michelle Crews

Dissertation

Submitted to the Faculty of the

Graduate School of Vanderbilt University

in partial fulfillment of the requirements

for the degree of

DOCTOR OF PHILOSOPHY

in

Physics

August, 2015

Nashville, Tennessee

Approved:

M. Shane Hutson, Ph.D.

Kirill I. Bolotin, Ph.D.

Jeffery M. Davidson, Ph.D.

Richard F. Haglund, Ph.D.

John P. Wikswo, Ph.D.

To my family,

your support made this possible.

ACKNOWLEDGEMENTS

There are so many people to acknowledge for helping me complete this dissertation. First, I would like to thank my family and friends who have supported me every step of the way. I could not have accomplished this without my husband Joe, who supported me through the long hours and late nights in the lab. Thank you to my parents, who have worked overtime as grandparents helping to watch my daughter Allison so I could concentrate on my work. I do not think I would be here if it had not been for the encouragement and support from my grandparents for my education. I would also like to thank my brothers, Andrew and Darren, for our continued sibling rivalry. Our competition helps drive me to be the best I can be. Thank you to my friend and sister-in-law, Susanne, for always being just a phone call away. I would also like to thank my office mate, Susan Kost, for letting me use her as a sounding board when I was stuck on a problem and for her encouragement and support.

I would also like to thank the members of my lab. I sincerely appreciate my advisor, M. Shane Hutson, for his enthusiasm and his dedication to making us all productive scientists. I owe a lot of credit for my training to Xiaoyan Ma, who took many hours helping me learn the ropes in the lab. Many thanks to the lab members who have graduated before me—Holley Lynch, Aroshan Jayasinghe, and David Mashburn—for all of your advice. I would especially like to thank Ty McCleery, who worked with me on the heat shock experiments. I was lucky to have such an enthusiastic and fun collaborator for what were often grueling experiments. I would also like to thank Monica Lacy and Alex Auner, for always being willing to lend a helping hand.

This work was funded through the GAANN fellowship, National Institutes of Health, and the Provost's Graduate Fellowship.

TABLE OF CONTENTS

LIST OF TABLES

Table Page

LIST OF FIGURES

CHAPTER 1

INTRODUCTION

Embryonic development is a complex process involving the coordinated movements of tissues and cells. While the innovations in molecular biology have allowed a great deal of characterization on the biochemical level of development, the description of development is not complete without an understanding of the underlying mechanics behind morphological events. The physics and the biochemistry are interdependent. The mechanical properties of the developing embryo inform the biochemistry, and changes in the biochemistry can alter the mechanical properties of the tissues.

The interdependence between the biochemistry and mechanics in biology also holds true when a system is exposed to an environmental stress. When a biological system is under stress, such as exposure to elevated temperatures, there is a switch from transcription of normal developmental proteins and an up regulation of the production of heat shock proteins—the heat shock response. The heat shock response is universal and has been observed from bacteria to humans. This project focuses on the mechanics of morphogenesis and how developmental mechanics are altered due to environmental stress, specifically heat shock, in *Drosophila melanogaster*. Understanding how the mechanics can be affected will give insight into the long term effects of environmental perturbations to development.

1.1 CELLULAR AND TISSUE MECHANICS

This work focuses on the developmental mechanics of two epithelial tissues, the amnioserosa and the germ band during *Drosophila* embryogenesis. The large morphogenetic movements of the amnioserosa and germ band require the coordinated activity of many inter- and intracellular components. These components determine the forces available to the tissues as well as the viscoelastic properties of the tissues that regulate motion. Figure 1 shows a simplified model of the epithelia. Each cell, encased by a plasma membrane, contains a nucleus and a network of filaments called the cytoskeleton. Above the germ band and amnioserosa cells there is a thin region filled with perivitelline fluid. There is a wax-coated membrane encasing the entire embryo called the vitelline membrane. Beneath the cells is a thin extracellular matrix. The cells are connected through adherens junctions, which are found near the apical surface of the cells.

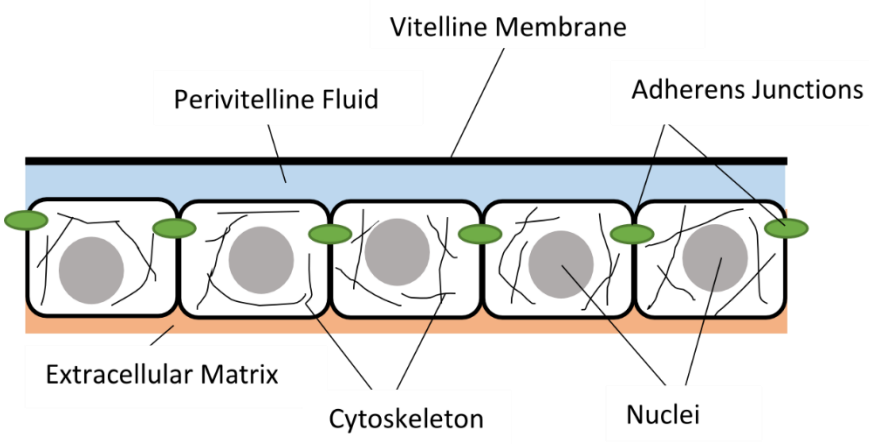

Figure 1. Simplified schematic of cuboidal epithelia in Drosophila embryogenesis.

1.1.1 THE CYTOSKELETON

The viscoelasticity and other mechanical properties of cells and cell sheets are determined by the underlying structure of the cells. During morphogenesis, the cells must adjust and reorganize to allow the cells to change shape. The cytoskeleton is responsible for cell shapes and shape changes and allows cells to withstand strains and stresses. There are three types of filaments that compose the cytoskeleton in cells: intermediate filaments for mechanical strength, microtubules to determine positions of organelles and for intracellular transport, and actin filaments which determine cell shape and movement (1). All of these filaments are dynamic and allow for quick changes when cell conditions change.

Filaments that comprise the cytoskeleton can span the length of cells, but because these filaments are composed of smaller subunits which can diffuse quickly, rapid rearrangement within a cell is possible. Intermediate filaments are made up of elongated and fibrous subunits, whereas actin filaments and microtubules are composed of compact and globular subunits called actin subunits and tubulin subunits respectively. These filaments bind together through weak non-covalent bonds, allowing for fast assembly and disassembly (1).

The actin filament subunit is a globular polypeptide chain which has a binding site for a nucleotide ATP or ADP. The subunits form polarized filaments as they attach head-to-tail. In the cell, these filaments become bundled and cross-linked by accessory proteins increasing the strength of the actin filaments. Actin filaments are usually nucleated in the plasma membrane of the cell. So, actin filaments are concentrated at the boundary of the cell and determine the shape and movement of the cell surface (1).

It is actin filaments that are responsible for the lamellipodia present during germ band retraction as the amnioserosa cells crawl over the germ band and the filopodia, or protruding bundles, that aid in the zipping of dorsal closure in *Drosophila* embryos.

Microtubule nucleation usually occurs in the center of the cell at the centrosome. From the centrosome, the microtubules branch out radially. This way the centrosome is in the center of the cell, and microtubules have access to position organelles throughout the cell. Intermediate filaments are not polarized like actin filaments or microtubules. Intermediate filaments pack together to build a rope-like element. This makes intermediate filaments flexible, but also strong. Figure 2 shows the relative strengths of the different types of filaments in the cytoskeleton.

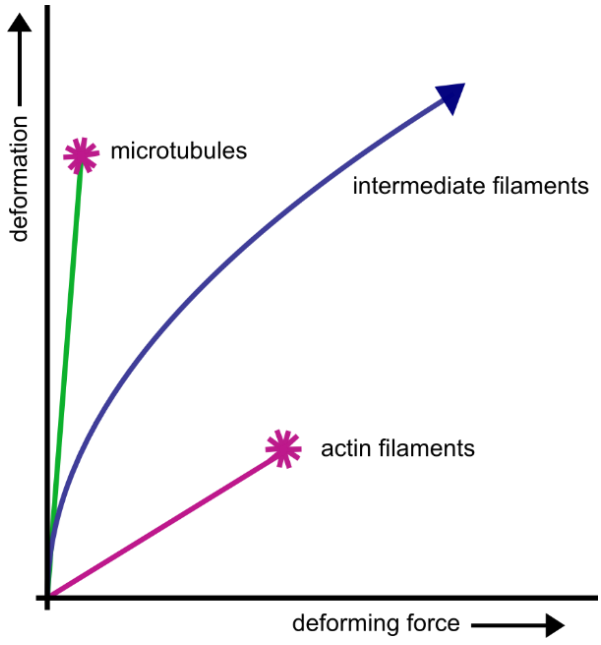

Figure 2. Relative strengths of cytoskeletal filaments. Microtubule filaments are easily deformed, but are also easily broken. Actin filaments are rigid, but also easily broken. Intermediate filaments are stronger and more flexible than both microtubule and actin filaments. Figure reproduced from (1)

The actin cytoskeleton of a cell is regulated by a family of GTPases called Rho GTPases. The Rho family of GTPases (GTP-binding proteins), which contains Cdc42, Rac, and Rho, relays signals from receptors on the cell surface to the actin cytoskeleton. These proteins act as molecular switches: active GTP-bound state and inactive GDP-bound state (1). Cdc42 activation results in actin polymerization and bundling for filopodia. Rac is important for actin polymerization of lamellipodial extensions and membrane ruffles. Rho activation causes bundling of actin filaments with myosin-II filaments into stress fibers (1). The results of microinjecting activated forms of Rho, Rac, and Cdc42 into a fibroblast cell are shown in Figure 3. Changes in the active levels of any of these three GTPases will affect the actin polymerization and cytoskeletal organization in a cell.

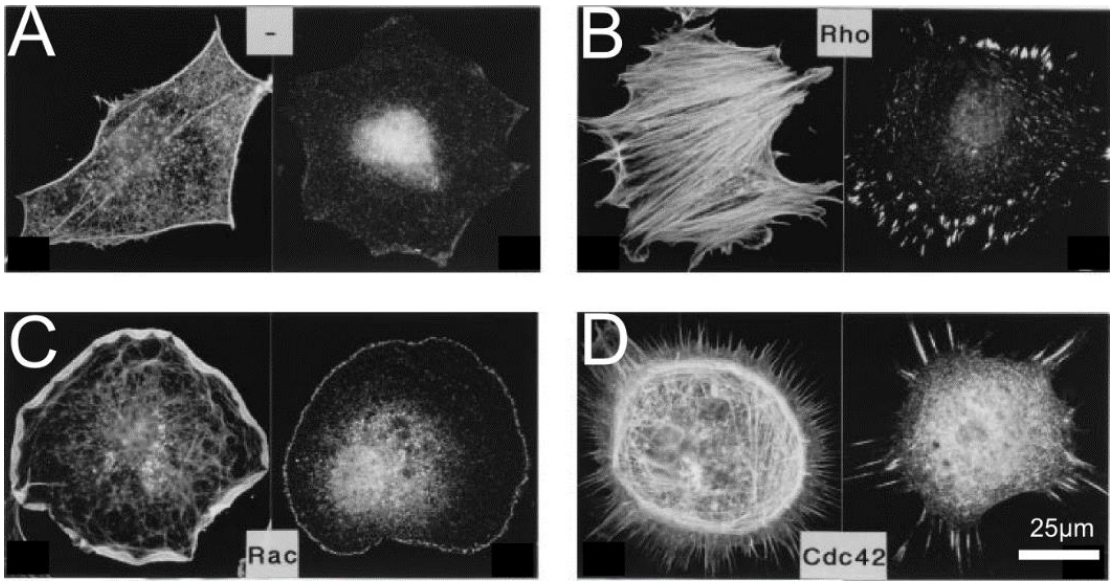

Figure 3. Rho, Rac, and Cdc42. (A) Actin staining (left) and vinculin staining to show focal adhesions (right) of fibroblast cell. (B) Fibroblast cell with injected activated Rho causes assembly of actin filaments and extra focal adhesion sites. (C) Fibroblast cell with injected activated Rac causes extension of lamellipodium. (D) Fibroblast cell injected with activated Cdc42 causes formation of numerous filopodia. Figure reproduced from (4).

Along the filaments in the cytoskeleton there are proteins that propel themselves using ATP hydrolysis. These proteins either carry organelles through the cell or slide filaments along each other generating force within the cell (1, 2). The motor protein, myosin, crawls along actin filaments. Myosin help with cell shape changes and are responsible for the contractile motion seen in amnioserosa cells during germ band retraction and dorsal closure. Cell shape changes are also regulated by the adhesion of cells with neighbors.

1.1.2 CELL-CELL ADHESION VIA ADHERENS JUNCTIONS

Epithelial tissues like the amnioserosa and germ band rely on adherens junctions to maintain cell-cell contacts and tissue integrity. The dynamics of the cytoskeleton along with the dynamics of adherens junctions allow for morphogenetic movements. Adhesion molecules that connect the cytoskeletons of neighboring cells are Ca^{2+}-dependent adhesion molecules called cadherins (Figure 4). E-cadherin, named for its presence in epithelia, is the primary adhesion molecule responsible for cell-cell adhesion in the amnioserosa and germ band during *Drosophila* embryogenesis. Cadherins are found on the apicolateral surface of epithelial cells (3).

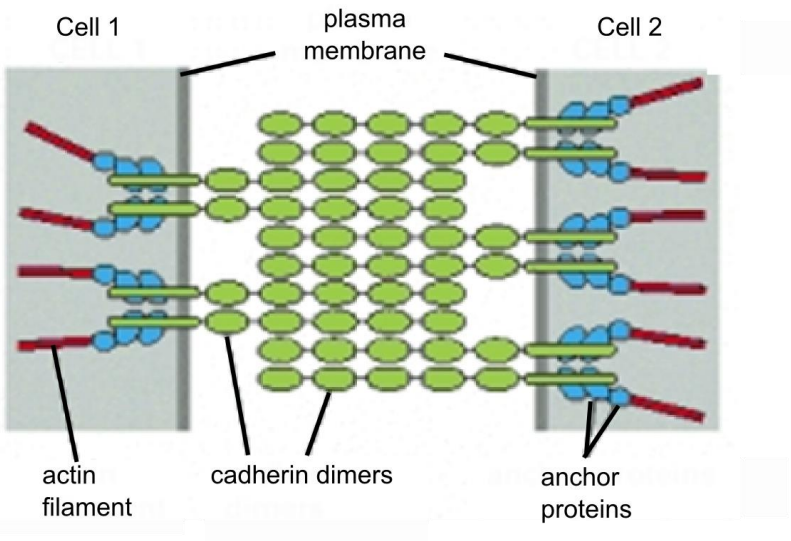

Figure 4. Cadherins. E-cadherin is the primary adhesion molecule responsible for cell-cell adhesion in the amnioserosa and germ band. Reproduced from (1).

1.2 DROSOPHILA MELANOGASTER

Drosophila melanogaster has been used extensively as a model organism. *Drosophila* is convenient in that stocks can be cheaply maintained and have quick generational turnover, taking approximately 2 weeks to develop from fertilized egg to mature adult. More importantly, *Drosophila melanogaster* has many genes that are homologous to human genes; 75% of human genes have related sequences in *Drosophila* (4). *Drosophila melanogaster* has been used to study diseases ranging from cancer to neurological or developmental disorders (3). It has also served as a model organism for studying a myriad of topics including signaling pathways, immunity, and wound healing. Because of the wealth of knowledge on the genetics and molecular biology of *Drosophila* development, *Drosophila melanogaster* is an ideal organism to

investigate not only the mechanical components of normal development, but also how the mechanics of development are altered after an environmental perturbation.

Bownes Stage	Minutes Post Fertilization	Description
1	0-15	Pronuclear fusion
2	15-70	Preblastoderm (mitotic cycles 1-9)
3	70-90	Pole bud formation
4	90-130	Syncytial blastoderm (mitotic cycles 10-13)
5	130-180	Cellularization of the blastoderm
6	180-195	Gastrulation
7	195-200	Germ band elongation
8	200-230	Rapid germ band elongation
9	230-260	Slow germ band elongation
10	260-320	Gnathal and clypeolabral lobe formation
11	320-440	Epidermal parasegmentation
12	440-580	Germ band retraction
13	560-620	End of germ band retraction
14	620-680	Dorsal closure, head involution
15	680-800	End of dorsal closure, head involution
16	800-900	Shortening of the ventral nerve cord
17	Until hatching	Tracheal tree fills with air

Table 1: Bownes stages of embryonic development. Times are given based on development at 25 ºC (4).

Drosophila melanogaster has a life cycle that lasts approximately two weeks as the animal develops from an embryo, to a larva, to a pupa, to a fertile adult. This work will focus on embryonic stages and will study the mechanics of two epithelial tissues during embryogenesis—the amnioserosa and the germ band—with specific emphasis

on the stages of germ band extension, germ band retraction, and dorsal closure. All of these movements are contained inside the ellipsoidal egg of the *Drosophila* embryos. *Drosophila* embryos have a length of approximately 500 µm and a minor axis of approximately 200 µm. Embryos are encased in a rigid chorion surrounding a wax-coated vitelline membrane (5).

Embryogenesis, lasting approximately 24 hours at room temperature (25 ºC), is broken down into seventeen Bownes stages (see Table 1)(6, 7) and involves the drastic, yet coordinated motion of the germ band and the amnioserosa. During the earliest stages (stages 1-4) of embryogenesis, nuclei in the embryo go through 13 rounds of synchronous mitoses and nuclei migrate to the perimeter of the embryo. By stage 5, two and a half hours into development, cell edges begin to form around the nuclei that are positioned along the perimeter of the embryo, forming a monolayer of cells around the inner yolk. The stage is now set for morphogenesis to begin.

1.2.1 GASTRULATION

By approximately three hours post fertilization, the embryo enters into Bownes stage 6, gastrulation. This stage, noted by the formation of the ventral and cephalic furrows (Figure 5), is when the embryo begins to form the mesoderm and endoderm, which will eventually form into the inner structure of the embryo. By this point in development, the embryo has already made the maternal to zygotic transition, where development has transitioned from being controlled by maternally deposited mRNA to the transcription of zygotic DNA (8). Although cell differentiation has been determined by the time gastrulation occurs, gastrulation is the first stage at which the different cell types become visibly apparent. The two main tissues that will be discussed in this work

are the amnioserosa and the germ band. The amnioserosa begins on the dorsal side of the embryo. At gastrulation, these cells have finished dividing and begin to change from columnar to squamous as their apical areas increase and the cells begin to elongate. The germ band cells, originating on the ventral portion of the embryo continue to go through several more rounds of mitosis, and the tissue begins to elongate around the posterior end of the embryo onto the dorsal surface, marking the initiation of germ band extension.

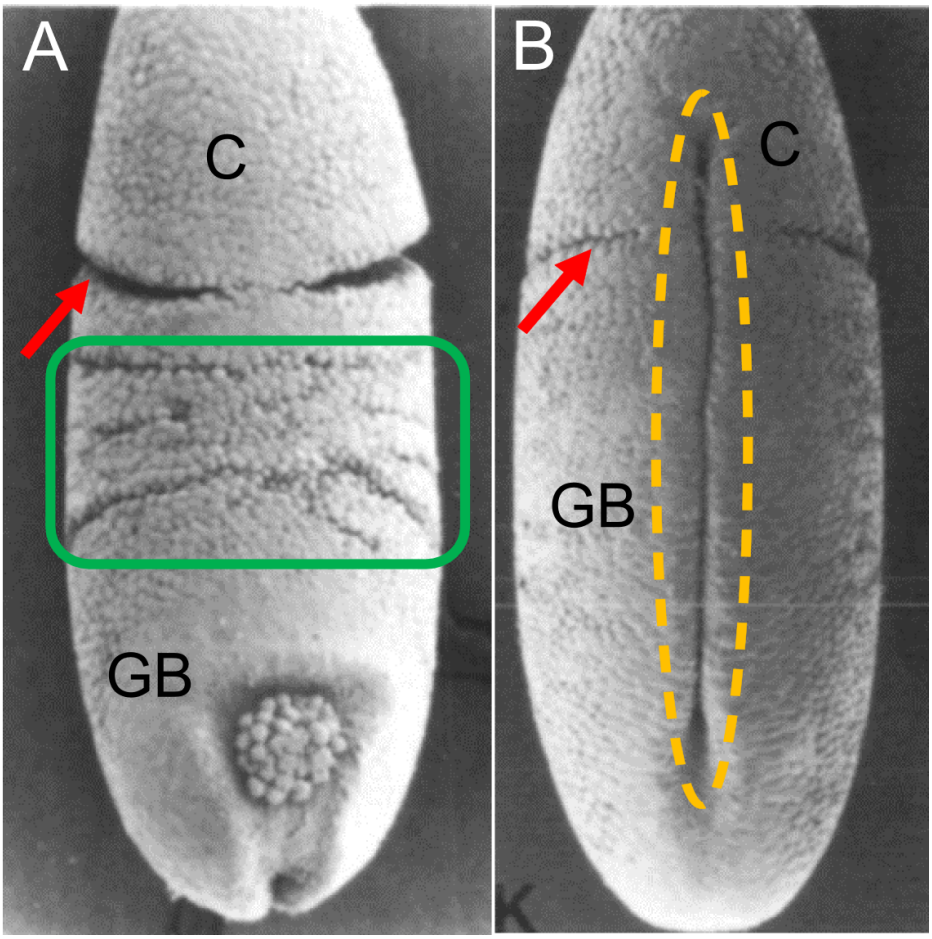

Figure 5. Gastrulation. (A) Dorsal view showing the cephalic furrow (red arrow) and the amnioserosa (circled in green); (B) ventral view of embryo showing cephalic furrow (red arrow) and ventral furrow (circled in yellow). Cephalic region is denoted by a "C" and the germ band is labeled "GB." Images reproduced from (9).

1.2.2 GERM BAND EXTENSION

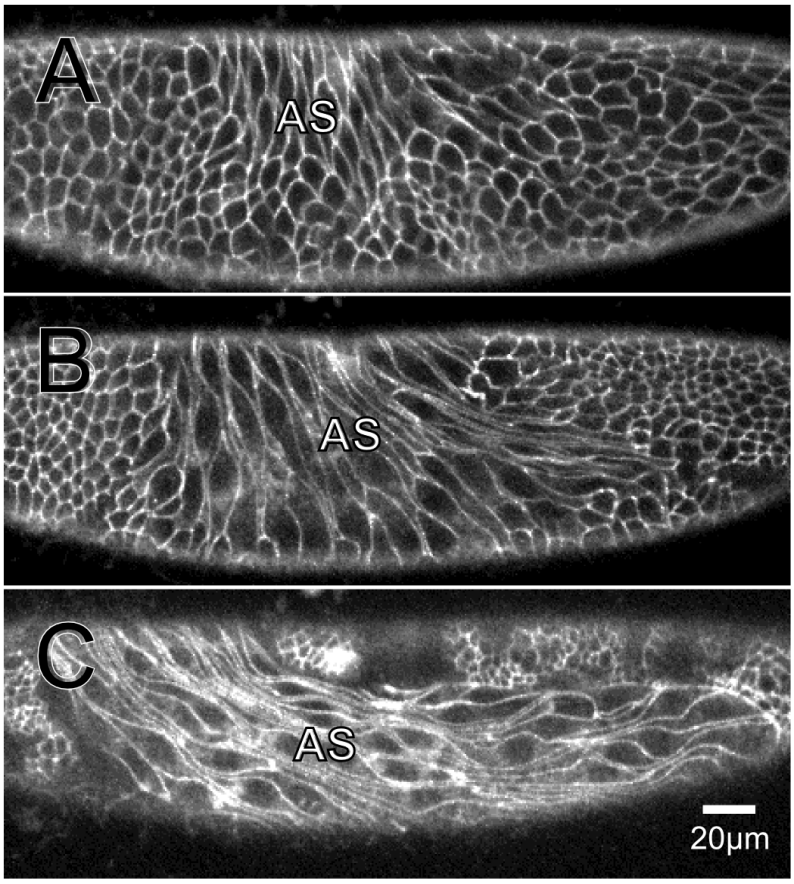

Figure 6. Confocal images of embryo during germ band extension. The amnioserosa cells elongate from (A) early (B) mid, and (C) late germ band extension

Germ band extension (Bownes stages 7-9) begins approximately 15 minutes after the start of gastrulation (Figure 6). During germ band extension, the amnioserosa cells, through rearrangement of microtubules and remodeling of adherens junctions, flatten and elongate into squamous cells (10). At the same time, the germ band elongates around the posterior end of the embryo onto the dorsal surface, increasing its length two and a half fold by convergent extension (11). The increase in tissue length is caused by intercalation of the germ band cells moving in between dorsal and ventral neighbors as shown in Figure 7 (11). By the end of germ band extension, the

amnioserosa cells are extremely elongated to an aspect ratio (defined as length divided by width of cell) of 11 and the germ band extends over much of the dorsal surface of the embryo (Figure 6C) (10). The embryo will pause in this position for stages 10 and 11 before the commencement of germ band retraction, the next major morphogenetic movement in *Drosophila* embryogenesis.

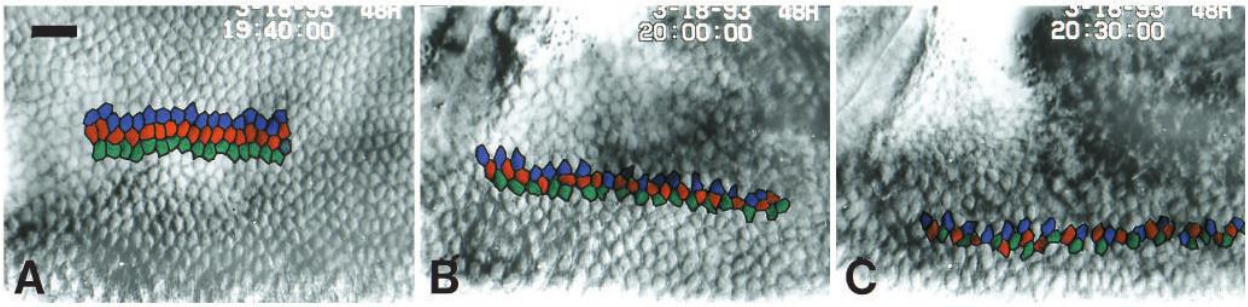

Figure 7. The germ band extends through cell intercalation. (A-C) Time lapse images showing dorsal and ventral neighbors (blue and green) move in between red cells to lengthen the germ band. Figure reproduced from (11).

1.2.3 GERM BAND RETRACTION

Germ band retraction (Bownes stages 12-13) begins 7 to 8 hours after fertilization and lasts 3 hours. Here, the germ band retracts back around the posterior end of the embryo as the amnioserosa cells become more isodiametric (Figure 8). This is accomplished not by cell rearrangement as seen during germ band extension, but rather by cell shape changes (12). During retraction, thoracic and abdominal segment boundaries form in the germ band, germ band cells elongate along their dorsal-ventral axis, and amnioserosa cells shorten. During retraction, amnioserosa cells extend

lamellipodia over the caudal end of the germ band (marked by a star in Figure 8), crawling over the germ band.

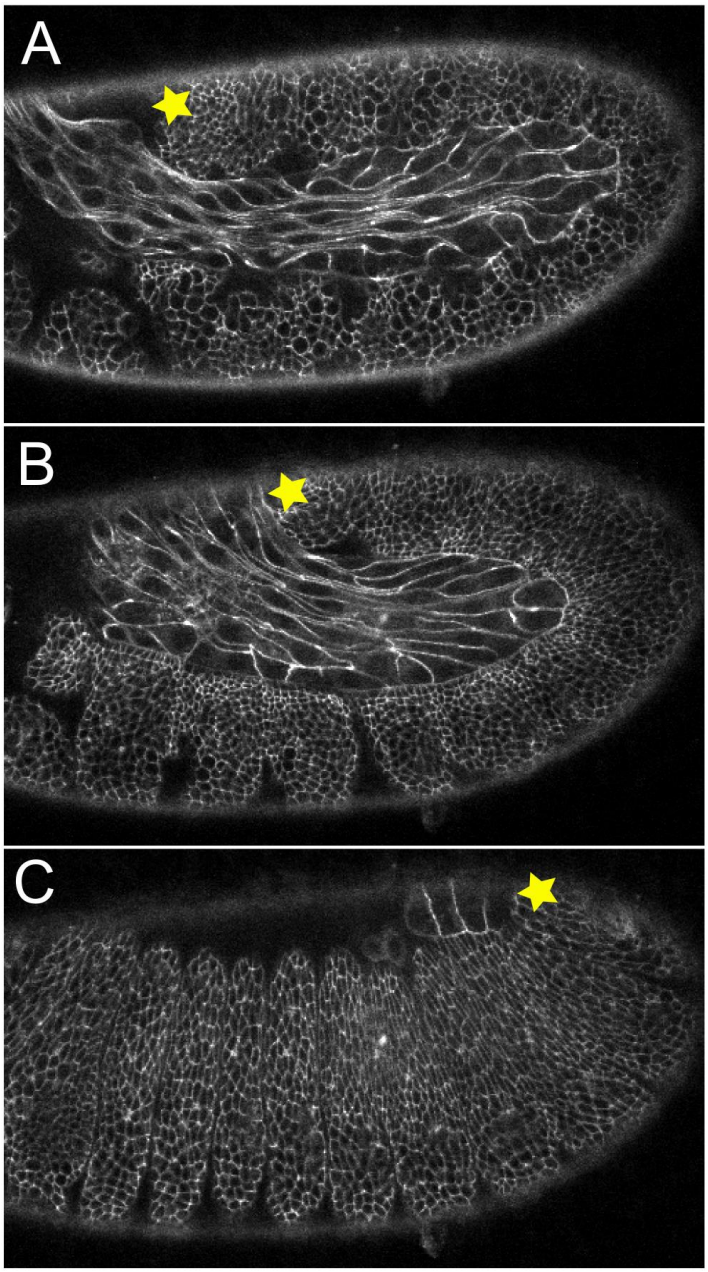

Figure 8. Confocal images of embryo during germ band retraction**.** Lateral view of (a) early, (b) mid, and (c) late retraction. The star marks the caudal end of the germ band.

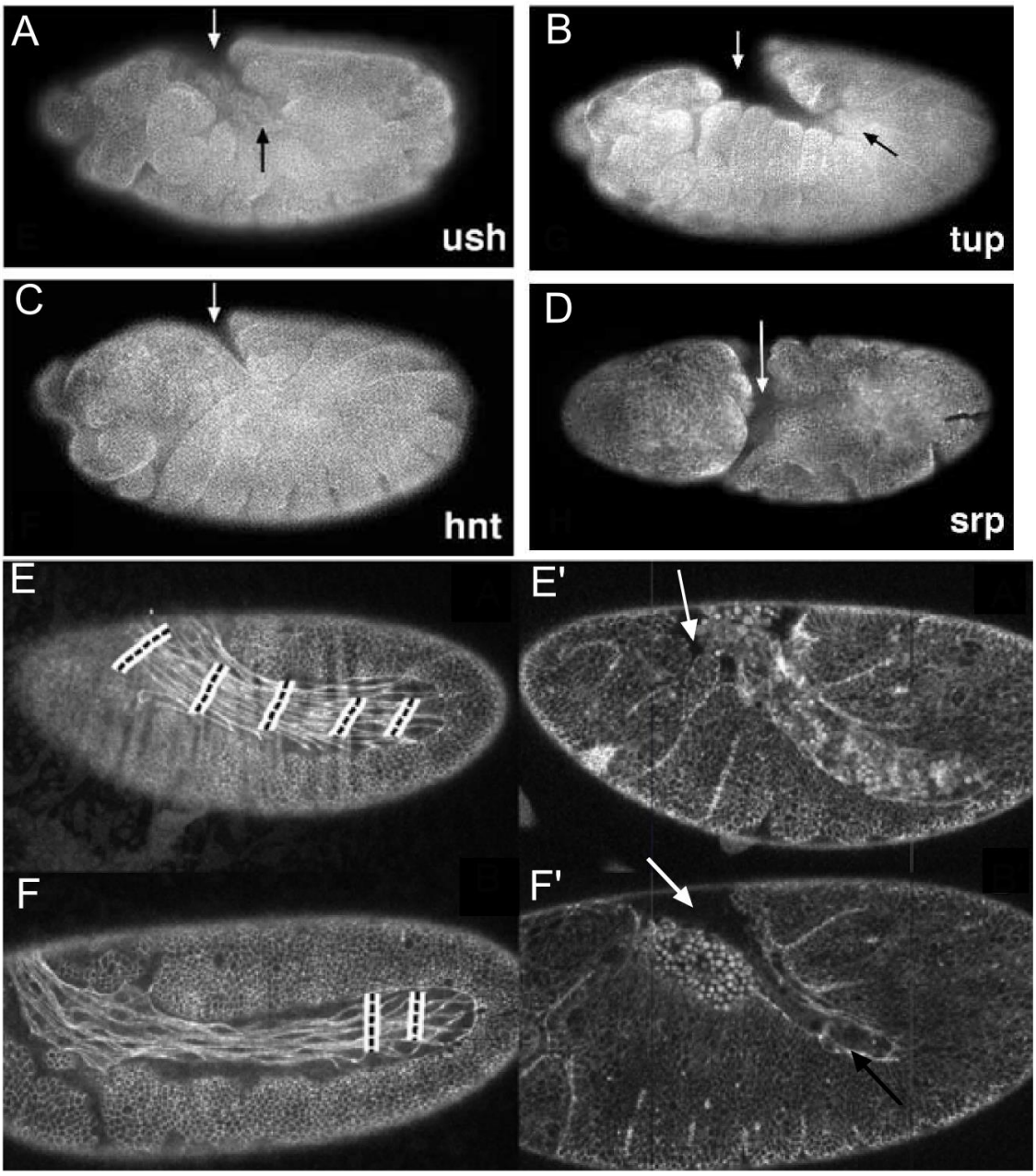

Figure 9: Failure of germ band retraction. *Ush* mutants fail to complete germ band retraction. (A-D) White arrows show the empty gap between the head and the germ band where the amnioserosa should be. Black arrows show left over amnioserosa cells. Ablations of the amnioserosa cause failure of germ band retraction (E-F) (13, 14).

The interplay between the amnioserosa and the germ band is essential for germ band retraction. This has been verified by the class of *u- shaped* mutants, named by the inability of the germ band to fully retract in these mutants, which leaves the germ band

in a permanent “u” shape (Figure 9A-D). In this class of mutants, integrity of the amnioserosa, which remains intact until dorsal closure in wild type development, is lost. The loss of the amnioserosa leads to a partial or complete failure of germ band retraction (13). The importance of the amnioserosa has also been established using laser microsurgery (14). Here, partial or complete destruction of one lateral side of the amnioserosa is enough to disrupt retraction. The mechanical contributions of amnioserosa and germ band cells to germ band retraction are discussed further in Chapter 2.

1.2.4 DORSAL CLOSURE

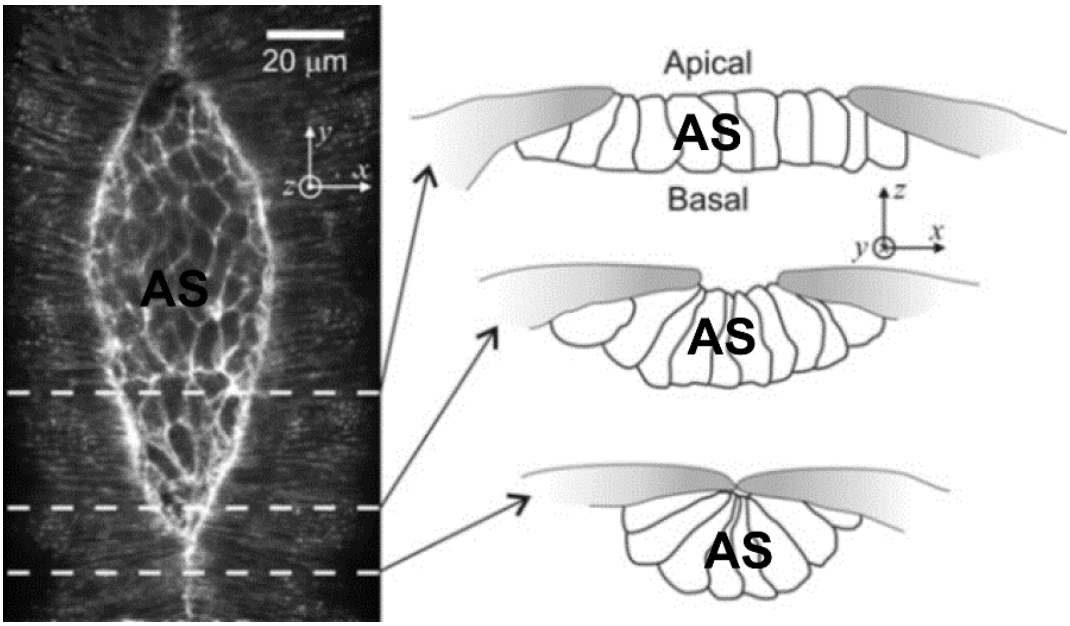

Figure 10. Dorsal closure. (Left) Confocal image of dorsal closure. Epidermal cells move over the amnioserosa. (Right) Amnioserosa cells contract their apical surfaces as closure proceeds. Figure reproduced from (15).

By approximately 12 hours post fertilization, the caudal end of the germ band has retracted to the posterior end of the embryo. This is the beginning of dorsal closure

(stages 14-15). By this point in development, the amnioserosa cells are isodiametric, and each cell is pulsing, periodically expanding and contracting its apical area. These pulsations occur while the germ band begins to zip up over the dorsal surface. As the zippering occurs, the amnioserosa cells become wedge-shaped (Figure 10) and begin to undergo apoptosis. After approximately 2 hours, the amnioserosa is no longer visible and the lateral epidermis covers the entire embryo.

1.3 HEAT SHOCK AND *DROSOPHILA* EMBRYOGENESIS

The heat shock response was first discovered in 1962 by Ferruccio Ritossa who noticed a new puffing pattern in the chromosomes of salivary glands in *Drosophila* larvae after exposure to a change in temperature (16) . The heat shock response has since been found to be a universal response—seen in organisms ranging from yeast to humans (17). The heat shock response is characterized by the halt of normal development and the switch to the transcription of heat shock proteins after a cell's exposure to stress. This stress does not have to be thermal, but can result from chemical or UV exposure or even from anoxia (18). The heat shock proteins are chaperone proteins and can aid in the folding of proteins, the movement of proteins, and the degradation of damaged proteins (18, 19).

Although the heat shock response helps to lessen damage to an organism from an environmental insult, stress at the wrong time during development can still result in serious developmental defects. The severity and type of defects in Drosophila embryogenesis as a result of heat shock depend on the timing and severity of the shock (20). These defects can range from minor defects in segmentation patterning to lethality. Interestingly, if a shock is administered at the onset of gastrulation, there are

developmental defects that do not develop until several hours after the shock and after normal gene transcription has resumed. Defects can be seen in germ band retraction, head formation, and segmentation (Figure 11) (20) leading to the question of how a non-specific environmental stress, like a heat shock, can alter the mechanics of the tissues in a developing organism. To understand the mechanics of how these defects happen, we must first understand the cell- and tissue-level mechanics of normal development. Subsequent chapters of this dissertation (Chapters 2-5) will describe both normal and perturbed mechanics.

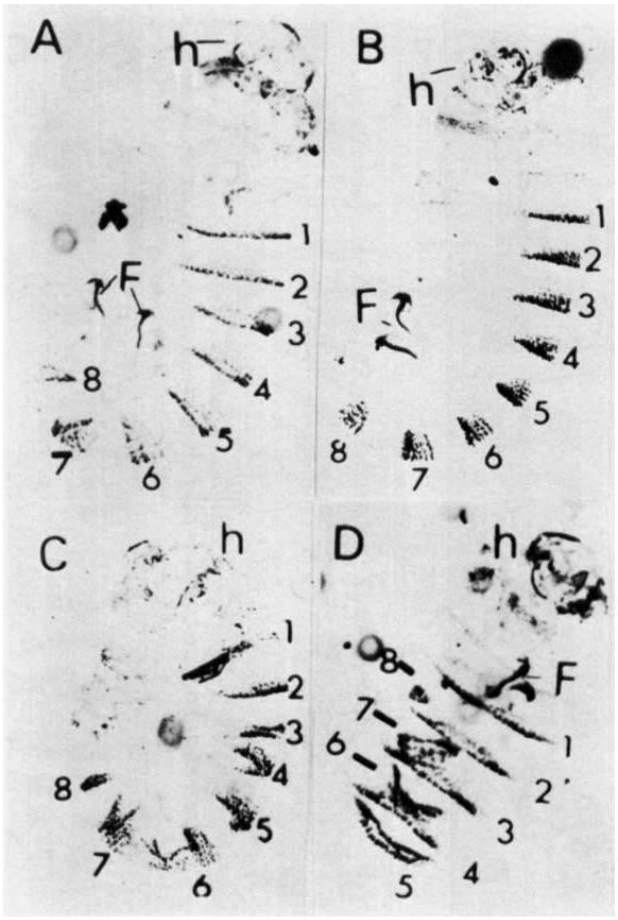

Figure 11. Developmental defects after gastrula heat shock. Cuticle stains from embryos heat shocked at gastrulation. The head is marked by an "h" and the caudal end of the germ band is labeled with "F." In these embryos, the germ band failed to fully retract evidenced by the position of the the caudal end of the germ band. Reproduced from (18).

The following chapter includes work published in

Lynch, Holley E., **Sarah M. Crews**, Brett Rosenthal, Elliott Kim, Robert Gish, Karl Echiverri, and M. Shane Hutson. "Cellular mechanics of germ band retraction in *Drosophila*. Developmental Biology 384 (2013) 205-213.

CHAPTER 2

CELLULAR MECHANICS OF GERM BAND RETRACTION

2.1 INTRODUCTION

Germ band retraction, a stage in *Drosophila* embryogenesis, involves the coordinated movements of two monolayered epithelial tissues—amnioserosa and germ band. At the beginning of germ band retraction, the germ band stretches from the ventral surface of the embryo, around the posterior end, and onto the dorsal surface. The amnioserosa is interlocked with the germ band, covering the lateral flanks of the embryo which are connected by a thin bridge of cells over the dorsal surface. As retraction proceeds, the germ band unfolds around the posterior end of the embryo as the amnioserosa cells move to cover the dorsal surface of the embryo. During this movement, the amnioserosa cells become more isodiametric, and the germ band cells elongate towards the amnioserosa. Distinct segments (T1-T2 and A1-A9) also form during retraction separated by the formation of furrows.

The amnioserosa has been shown to be mechanically essential for retraction to take place (13, 14, 21–23). In a group of mutants where the amnioserosa undergoes premature apoptosis or is otherwise lost (*u-shaped*, *serpent*, *hindsight*, and *tail-up*),

germ band retraction fails (13). Loss of half of the amnioserosa through laser ablation is also sufficient to cause a failure of germ band retraction (14). Although is it clear that the amnioserosa plays an essential role in germ band retraction, it is unclear how much of a role the amnioserosa plays in the cell-level shape changes in the germ band. To what extent are these cell shape changes in the germ band a result of forces from the amnioserosa? To what extent are germ band cells elongating autonomously? Here we test the hypothesis that cell shape changes in the germ band are a passive result from being pulled on by the amnioserosa as the germ band unfolds.

Using a combination of laser microsurgery and careful quantification of cell shape changes, we worked to decipher the contribution of the amnioserosa to cell shape changes in the retracting germ band. Our results suggest that mechanical interactions between the amnioserosa and germ band are subtle. Many cell shape changes in the germ band are mechanically autonomous, but complete unfurling of this tissue clearly requires a mechanical assist from the amnioserosa.

2.2 MATERIALS AND METHODS

2.2.1 FLY STRAINS

The primary *Drosophila melanogaster* strain used in these studies was *ubi-DE-Cad-GFP* (24) (*Drosophila* Genetic Research Center, Kyoto, Japan), which ubiquitously expresses E-Cadherin-GFP to label epithelial cell junctions. Where noted, we used the strain *sGMCA-3.1* (3rd chromosome insertion; gift from DP Kiehart, (25)) to label actin filaments. Cell shapes in u-shaped (*ush*) mutants (13) were analyzed by secondary

antibody staining of unretracted embryos collected from a *ush*^{2} *cn*^{1} *bw*^{1} *sp*^{1}/*CyO* stock (Bloomington Stock Center, Bloomington, IN).

2.2.2 SLIDE PREPARATION AND LIVE EMBRYO IMAGING

Slides of 20-30 embryos from two-hour collections were made following a modified version of previously published procedures (26). After collection, embryos were kept at approximately 15 °C until reaching germ band retraction. Some embryos were used directly after this incubation period, others were stored for a few hours at 4 °C to halt development, and later warmed during slide preparation back to room temperature. No differences were detected. Embryos were dechorionated in a 50% bleach solution, arranged on their lateral side and mounted to a cover slip using embryo glue. The embryos were left uncovered on the slide for approximately 3 minutes before being covered in halocarbon oil 27 (Sigma-Aldrich, St Louis, MO). This exposure lead to a slight dehydration that enabled flattening of the embryo, allowing more complete lateral images on a confocal system without using multiple depth slices. The embryos were finally mounted in a metal slide between the cover slip and an oxygen permeable membrane (YSI, Yellow Spring, OH). Images were captured using a Zeiss LSM410 laser-scanning confocal microscope (inverted) with a 40×, 1.3 NA oil-immersion objective. The scanning time was 8 s per frame.

2.2.3 IMMUNOFLUORESCENCE MICROSCOPY OF FIXED EMBRYOS

For immunofluorescence of *ush* mutants, embryos from the balanced *ush/CyO* stock were collected as above, aged for a time normally equivalent to Bownes stage 14, fixed in methanol, stained with monoclonal mouse anti-α–Spectrin (Antibody 3A9,

Developmental Studies Hybridoma Bank, University of Iowa), and then with Alex Fluor 488 donkey anti-mouse IgG (Molecular Probes, Life Technologies, Grand Island, NY). These embryos are a Mendelian mix of *ush/ush*, *ush/CyO* and *CyO/CyO* – the latter viable through late embryogenesis (27, 28). Presumptive *ush/ush* embryos are identified from confocal images as those with an unretracted phenotype and no remaining amnioserosa cells.

2.2.4 LASER MICROSURGERY SYSTEM

Laser microsurgery was conducted using the above confocal microscope coupled with the 3rd harmonic (355 nm) of a Q-switched Nd:YAG laser (5 ns pulse width, Continuum Minilite II, Santa Clara, CA). The ablating laser was targeted to specific regions of fly embryos using a computer-controlled steering mirror and a custom plug-in for ImageJ (NIH, Bethesda, MD). This plug-in allows users to draw various shapes on a recently obtained image and directs the ablating laser along the user-defined path. Extended incisions were created using multiple pulses with the physical distance between ablation sites controlled by the steering mirror's scan speed. At a 10-Hz repetition rate, achieving smooth cuts required slow scanning speeds, ~2 s for a 15-µm line.

2.2.5 DEVELOPMENTAL STAGING VIA CONTOUR MATCHING

Embryos' progress through germ band retraction were staged using a contour-matching staging algorithm was developed by Holley E. Lynch and M. Shane Hutson described in (14). Briefly, this method uses a least squares regression algorithm to find the best alignment of the contour of the amnioserosa-germ band boundary from the

interface between segments T3/A1 to that between segments A7/A8 (Figure 12 A,B) to a standard set allowing for rotation, translation, and scaling. Contour alignments for staging were run using Mathematica (Wolfram Research, Champaign, IL).

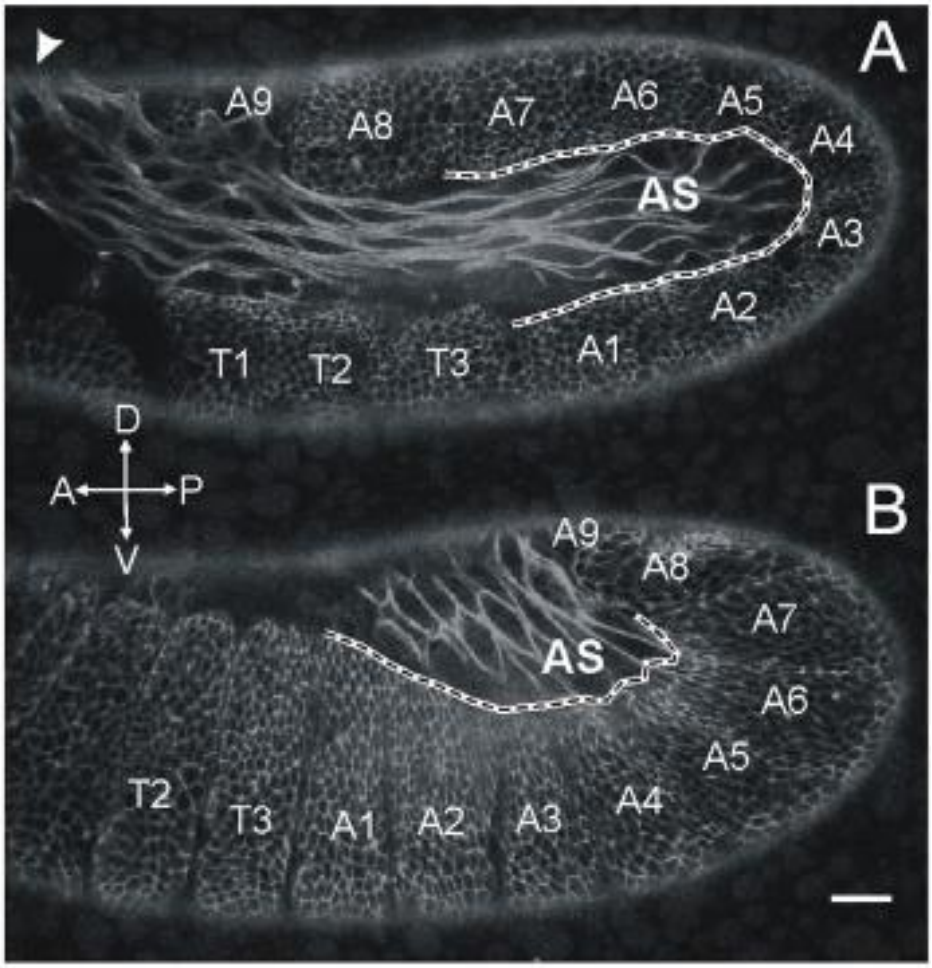

Figure 12. Contour staging method. (A) Lateral view of an E-cadherin–GFP embryo in early germ band retraction showing a staging contour (black dashed line surrounded by white) that follows the amnioserosa-germ band interface from segment boundary T3/A1 to A7/A8. The white arrows denote global anterioposterior (A–P) and dorsoventral (D–V) axes. The white arrowhead at top left denotes the thin bridge of cells that connects the two lateral flanks of amnioserosa. (B) Similar view and staging contour for an embryo in late germ band retraction. Scale bar represents 20µm (14).

2.2.6 ANALYSIS OF CELL SHAPE AND ALIGNMENT

Images were segmented to analyze cell shape using SeedWater Segmenter (29). We tracked cell shape changes via both the average cellular aspect ratio and a cellular area moment of inertia tensor (30),

$$\boldsymbol{J} = \sum_i \begin{bmatrix} y_i^2 & -x_i y_i \\ -x_i y_i & x_i^2 \end{bmatrix} \Delta x_i \Delta y_i \tag{7}$$

where x_i and y_i are the coordinates of a single pixel (relative to the cell's centroid), Δx_i and Δy_i are the dimensions of that pixel, and the sum is taken over all image pixels i belonging to a single cell. This $\boldsymbol{J}$ tensor maintains information on cellular orientation that is lost in a simple averaging of aspect ratios. For example, the rotation that diagonalizes this tensor (to $\boldsymbol{J}'$) yields the direction of one of the cell's principal axes (equivalent to the axes of its best-fit ellipse). We take α as the direction of the cell's longest principal axis and track cell elongation through the ratio of the cell's extension along its two principal axes

$$\kappa = \sqrt{\frac{\boldsymbol{J'}_{\boldsymbol{max}}}{\boldsymbol{J'}_{\boldsymbol{min}}}} \tag{8}$$

where $\boldsymbol{J'}_{\boldsymbol{max}}$ is the largest diagonal entry in the rotated $\boldsymbol{J}'$ tensor and $\boldsymbol{J'}_{\boldsymbol{min}}$ is the smallest diagonal entry. κ is equal to the aspect ratio of a cell's best-fit ellipse. The $\boldsymbol{J}$ tensors for multiple cells can be averaged together and then used to calculate α and κ for a composite cell. This averaging at the tensor level maintains a dependence on the elongation direction, *e.g.*, if all the cells had individual aspect ratios of two and all were

aligned in the same direction, then the composite κ would also be two, but if the cells were randomly oriented, then the composite κ would be close to one. Tracking both κ and mean aspect ratio enables a more complete description of cell shape and orientation changes. Note that the reported angles α are calculated based on the local segment coordinates. Thus, an angle has the same meaning within the segment regardless of the segment's current position in the embryo. Post-segmentation analysis of cell shapes was also conducted using Mathematica (Wolfram Research, Champaign, IL).

2.2.7 IMAGE ANALYSIS

Routine analysis and image adjustments, *e.g.*, brightness/contrast and inversion, were performed in ImageJ (NIH, Bethesda, MD).

2.3 RESULTS

2.3.1 EXTERNAL FORCES ON THE GERM BAND

If the amnioserosa plays an active mechanical role in germ band retraction, then segments of the germ band should experience an external force in the direction along which the amnioserosa contracts. Using laser microsurgery, Holley Lynch *et al*. (14) made small incisions in each segment of the germ band and examined the tissue response. The assessment was done such that each segment has a local coordinate system where the *y*-direction is defined to stretch from the edge of the embryo to the amnioserosa (Figure 13C-inset, red arrows), bisecting the angle between the segment's

boundaries; the *x*-direction is perpendicular to that (Figure 13C-inset, blue arrows). The positive *x*-direction is in the direction of segment motion (caudal to rostral) and the positive *y*-direction is in the direction of the amnioserosa.

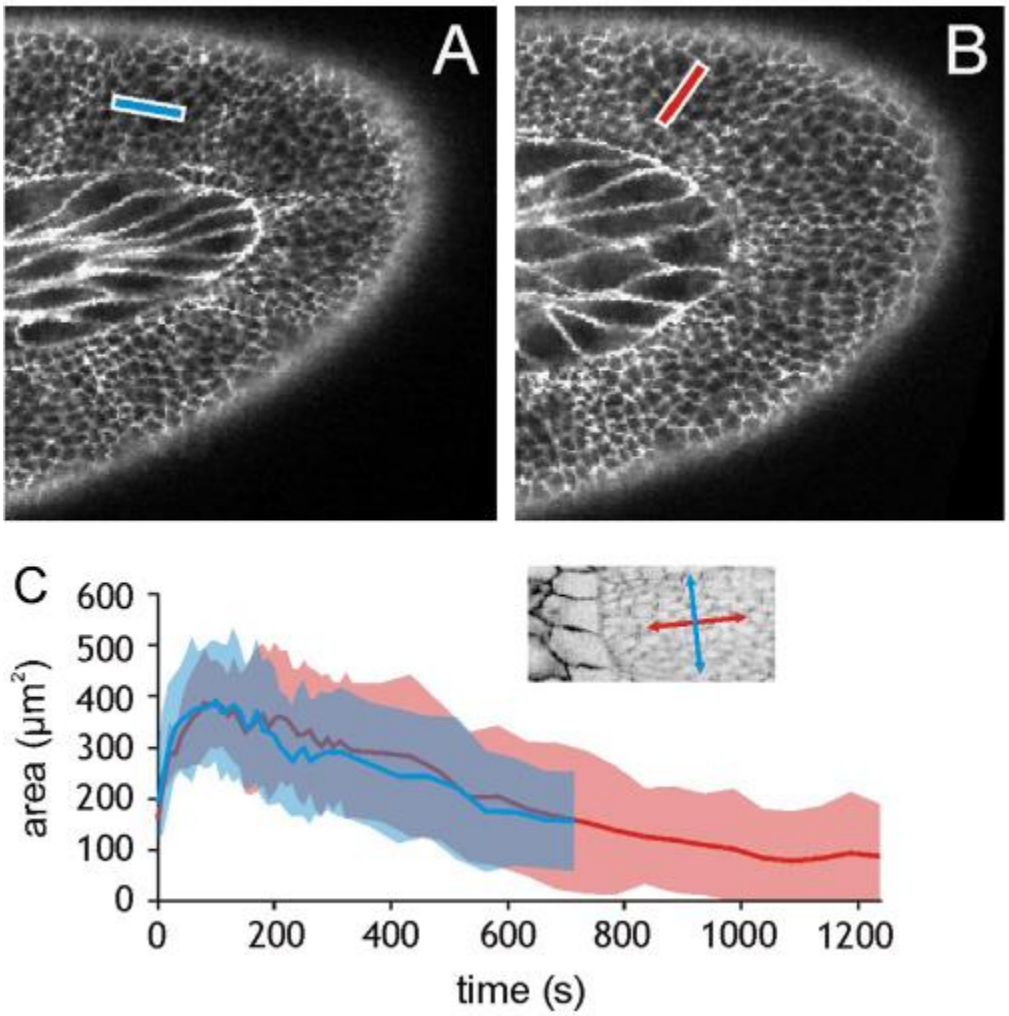

Figure 13. Orientation of linear incisions in the germ band. (A) Targeted area for a 15-μm long laser incision along the x-axis of segment A5. (B) Same along the y-axis of A5. (C) Dynamics of wound area versus time for incisions along the x- (blue) and y- (red) axes of segment A7 as mean (solid lines) ± one standard deviation (shaded areas). This graph is typical for both directions in all segments. The inset shows the orientation of segment-specific x- (blue) and y- (red) axes.

Lynch, *et al.* examined how the tissue reacts to small laser incisions by making 15-μm line cuts in embryos during germ band retraction along the *x*- and *y*- direction in

each segment (Figure 13A, B respectively). In response to each incision, the tissue recoils from the ablation site, the wound reaches a maximum area, and then begins to heal (Figure 13C). In all segments, both wound types opened to comparable sizes; however, in segments A4, A5, and A7, which spend a large amount of time in the bend of the germ band, there was a statistically significant difference in aspect ratio between wounds due to incisions in the x- versus y-directions. The largest aspect ratios were observed in cuts made in the y-direction (towards the amnioserosa).

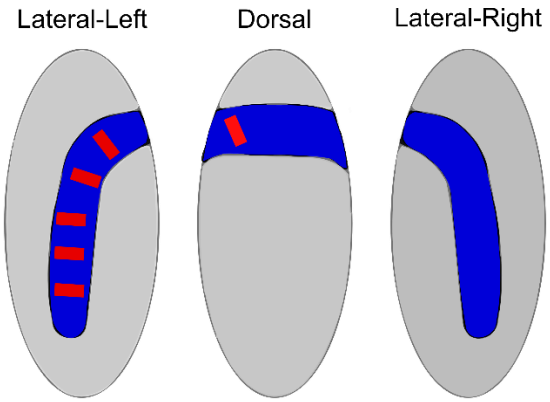

Figure 14: Diagram of embryo. Only one flank of the amnioserosa (Blue) is ablated. Ablation lines are represented in red. The other half (Lateral-Right) of the amnioserosa remains intact.

These results suggest the hypothesis that anisotropic stresses in segments A4, A5 and A7 are caused by forces exerted on the germ band by the amnioserosa. To test this hypothesis, we made additional linear incisions in segment A5 just after ablation of one flank of the amnioserosa (See Figure 14). These linear incisions opened up to mean areas and perimeters similar to those above, but their aspect ratios were different. After amnioserosa ablation, the mean ± one standard deviation for incisions along the *x*-axis of segment A5 was 1.00 ± 0.42 (N = 6), and that for incisions along the *y*-axis was

1.65 ± 0.52 (N = 5). Ablating half the amnioserosa thus leads to a fairly strong reduction in the anisotropy of wounds along the y-axis of segment A5, which was 2.29 ± 0.28 when the amnioserosa was intact. With this reduced anisotropy and with the larger variances observed after amnioserosa ablation, the shapes of wounds along the x- and y-directions were not significantly different. The p-value for this comparison is borderline (p = 0.055), so although these results support a model in which stress anisotropy in the germ band arises from forces generated in the amnioserosa, they do so only weakly. The complex wound healing response initiated around the ablated flank of amnioserosa prohibits this experiment from being more conclusive.

2.3.2 GERM BAND CHANGES IN THE ABSENCE OF RETRACTION

To test the autonomy of the cell shape changes in the germ band during retraction we ablated half of the amnioserosa and then tracked its impact on cell shape changes in the germ band. At the start of retraction, cells in the curve of the germ band and along its ventrolateral aspect are only slightly elongated: <aspect ratio> = 1.57 ± 0.06 and $< \kappa >$ = 1.15 ± 0.11 at a staging of <R> = 6 ± 19% retraction (N = 2 segments in each of 5 embryos with 20-50 cells per segment). The mean composite κ is lower than the mean aspect ratio because the cells are only weakly aligned. By the end of germ band retraction (<R> = 90 ± 12%), the cells become more elongated and more strongly aligned: <aspect ratio> = 1.72 ± 0.18 and $< \kappa >$ = 1.39 ± 0.12. This trend is also evident in the rose diagrams of the control group in Figure 15. In later stages of retraction, more cells are oriented with their long axis towards the amnioserosa (more darkly shaded sectors near 90°) and these cells have longer aspect ratios (increased length of these sectors).

Although cells in control embryos elongate and align similarly in segments A2 and A5, these segments behave very differently when the amnioserosa is ablated. After ablation of one flank of the amnioserosa, elongation and alignment in segment A2 is nearly eliminated. The mean aspect ratio and mean composite κ themselves give no indication of elongation (<aspect ratio> = 1.47 ± 0.02 and $< \kappa >$ = 1.16 ± 0.11 for N = 5 embryos with $<R>$ = 92 ± 9%), and the corresponding rose diagram in Figure 15 has sectors near 90° that are only slightly longer and darker. Looking at the individual experiments, post-ablation alignment of cells in segment A2 was only evident in two of five embryos.

On the other hand, despite ablation of the amnioserosa, cells in segment A5 elongate and align normally: <aspect ratio> = 1.76 ± 0.05 and $<\kappa>$ = 1.45 ± 0.08 for N = 5 embryos with $<R>$ = 87 ± 14%. This indicates that cell elongation occurs normally for a segment along the germ band's curve, even without a complete amnioserosa, and even in the absence of retraction. The late stage rose diagrams for segment A5 in control and ablated embryos differ only by a slight shift in the alignment direction (last column of Figure 15), but inspection of the individual experiments shows that this shift is primarily due to a very large alignment shift in just one of five embryos.

These results provide an interesting contrast with the results from stress anisotropy measurements in the germ band. During mid-retraction, segments in the curve of the germ band have high stress anisotropy – with large tensile stresses in the direction of the amnioserosa – but ablation of the amnioserosa has almost no effect on these cells' elongation and alignment. In a nearly opposite fashion, segments along the ventrolateral aspect of the germ band display low stress anisotropy, but their elongation

is highly dependent on having an intact amnioserosa. These results are at odds with a simple model in which tension from the amnioserosa helps elongate and align germ band cells, and ablation of the amnioserosa simply removes this normally assistive tension.

One obvious complication of these ablation experiments is their limitation to removing just half the amnioserosa. For comparison, we imaged *ush* mutant embryos with an unretracted phenotype in which the amnioserosa dies prematurely. Using a balanced *ush/CyO* stock, the Mendelian mix of embryonic genotypes allowed use of presumably wild-type and heterozygous embryos to gauge the collection's approximate developmental stage. By waiting long enough for most embryos to progress into mid dorsal closure (stage 14), there was a clearly identifiable minority of embryos that remained unretracted. Confocal images of unretracted embryos that were fixed and stained with anti-α-Spectrin antibodies showed a complete absence of amnioserosa cells and almost no elongation or alignment of germ band cells (Figure 15C-E). Cells in segment A5 did not elongate beyond what was normally observed in early germ band retraction (<aspect ratio> = 1.50 ± 0.05 and $< \kappa >$ = 1.11 ± 0.08 for N = 5 embryos) and those in segment A2 barely elongated (<aspect ratio> = 1.59 ± 0.12 and $< \kappa >$ = 1.29 ± 0.16 for N = 5 embryos). These results are clearly different from what we observed after ablation of the amnioserosa – most notably in segment A5. The implications of these differences are discussed in detail in the Discussion.

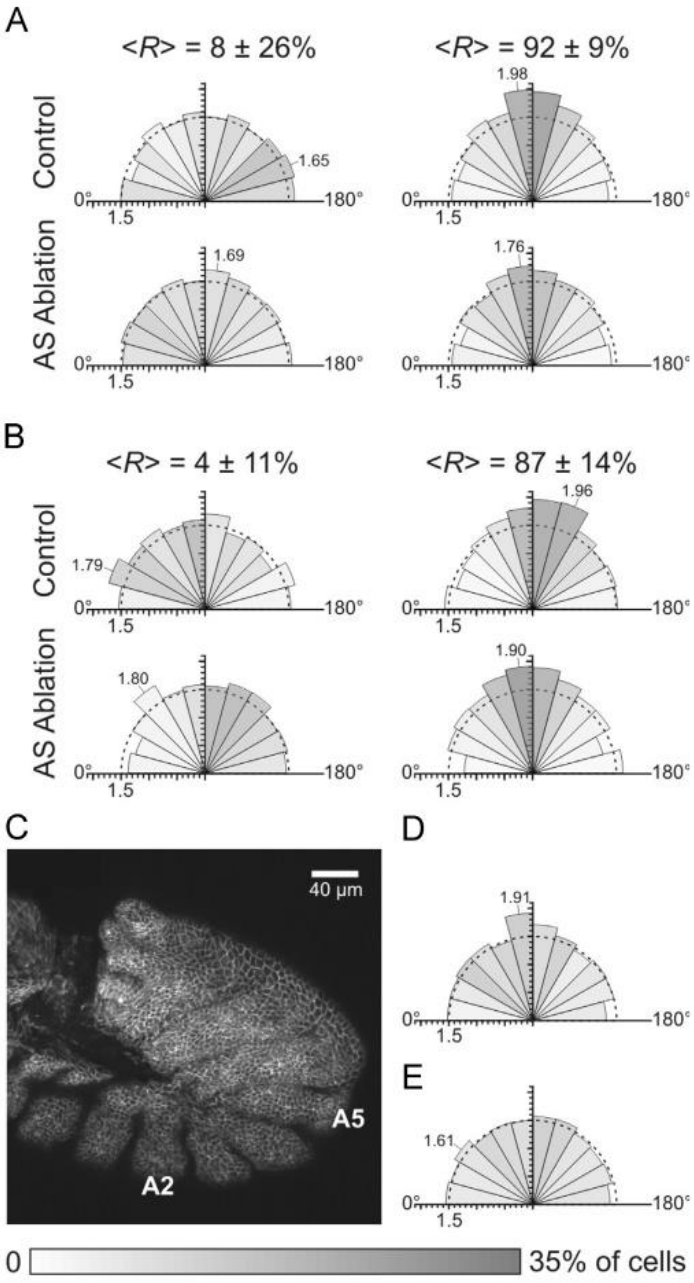

Figure 15. Dynamic elongation and alignment of germ band cells in normal, laser-perturbed and *ush* mutant embryos. Each rose diagram compiles data from N=5 embryos to detail cell shape and orientation. The shading of each sector represents the fraction of cells aligned in a particular direction – darker for larger fractions (grayscale bar at the bottom of the figure). The length of each wedge is proportional to the mean aspect ratio of cells aligned within that sector. An aspect ratio scale is provided by tick marks on the radial axis, a semicircle at a mean aspect ratio of 1.5, and labeling of sectors with the most elongated cells. An angle of 90 degrees represents alignment of cells towards the amnioserosa, i.e., along the local y-axis. (A, B) Dynamic cell shape changes tracked in segments A2 (A) and A5 (B) from early to late germ band retraction and in both control embryos and those in which one flank of the amnioserosa was ablated. The range of stages (R=% retraction) included in each control group is noted above each rose diagram as the mean ± one standard deviation. Control embryo images were stage-matched to the ablated embryo images based on pre-ablation stage and the elapsed time between pre- and post-ablation images (1–2 h). (C) Confocal fluorescent image of a *ush/ush* embryo with anti-α-Spectrin staining. Scale bar is 40 µm. Although this embryo should have progressed to stage 13 or 14, it shows no evidence of any remaining amnioserosa cells and its germ band is unretracted. (D, E) Rose diagrams of cell elongation and alignment in ush/ush embryos that failed to complete germ band retraction. There is very weak alignment of cells in segment A2 (D) towards where the amnioserosa would have been (near 90º) and essentially no extension or alignment of cells in segment A5 (E).

2.4 DISCUSSION

Our experiments give conflicting results. Ablation experiments support the hypothesis that amnioserosal forces are not the sole driver of germ band retraction, but are instead assistive – at least under normal mechanical conditions. Some germ band cells elongate normally even after ablation of one flank of the amnioserosa (Figure 15b) – which could be interpreted as a germ band autonomous contribution. In contrast, germ band cells do not elongate normally in *ush* mutants in which the entire amnioserosa dies prematurely (Figure 15E).

When comparing these two experiments, it is important to recognize the differences and how these differences could impact the results. While both laser ablation of one half of the amnioserosa and the premature death of the amnioserosa in *ush* mutants are sufficient to cause failure of retraction, the response within the embryo is not exactly the same. The laser ablation experiments will induce a wound healing response that can alter the pattern of stress fields and the activation of biochemical signaling pathways in surrounding tissues. Additionally, half of the amnioserosa is still intact after the laser ablation experiments, which causes the embryo to twist. This is especially evident for cells in the crook of the germ band, some of which move around the posterior end of the embryo towards the other flank of intact amnioserosa. In *ush* mutants, such twisting is seen, but only occasionally. We do not have live imaging of *ush* mutants to see whether this occasional twisting occurs when there is asymmetric cell death in the two flanks of amnioserosa, but that is certainly what one would expect.

Ablation of half the amnioserosa suppresses elongation of ventrolateral germ band cells (Figure 15A, segment A2), but allows near normal elongation for those in the

crook of the germ band (Figure 15B, segment A5). Oddly, cells normally subjected to the largest pulling forces from the amnioserosa (A5) are the ones that actually elongate most after ablation of half the amnioserosa. In contrast, the unretracted phenotype of *ush* mutants is associated with a near complete loss of elongation for cells in both segments A2 and A5 (Figure 15D-E). In fact, the little remaining elongation is stronger in A2 than in A5, opposite what is observed after ablation.

We suggest that the apparent contradiction is traceable to an oversimplification of the tissue mechanics after ablation of just half the amnioserosa. Because the other lateral flank of amnioserosa remains intact, such ablations do not simply remove amnioserosa tension, but instead strongly disturb the normal pattern of tensile stress. The new pattern would lead to twisting of the germ band, continued anisotropic tension in segments A4-A7 (strongest in the local *y*-direction), and increased tension along the *x*-direction of ventrolateral segments T1-A3. Cells in segment A5 would still be subjected to a stress anisotropy in the *y*-direction and thus extend and align normally. Cells in segment A2 would now be subjected to an aberrant stress in the local *x*-direction that suppresses their normal *y*-directed elongation. This hypothesis could be tested in the future by computational modeling, video force microscopy or long-term double-ablation experiments in which anisotropy is probed in more than just segment A5 long after removal of half the amnioserosa. Even without such tests, it is clear that ablation of just half the amnioserosa poorly recapitulates *ush* mutants. Both convey important information about the role of amnioserosa cells in germ band retraction, but they are not equivalent.

Our observations suggest an interesting model for germ band retraction, one in which both tissues play a role. Successful germ band retraction clearly requires mechanical integrity of the amnioserosa. This requirement does not exclude additional juxtacrine and/or paracrine signaling roles, but the amnioserosa generates critically important forces. Nonetheless, these forces do not directly assist cell shape changes in all segments of the germ band. In some, particularly those in ventrolateral regions, the mechanical role of the amnioserosa is more permissive – its intact presence prevents aberrant patterns of mechanical stress that can prevent normal cell elongation. Together these results lend credence to a model where some of the germ band changes are mechanically autonomous, but where the amnioserosa is anchored to the caudal end of the germ band, contracts dorsoventrally, and thus assists uncurling of the germ band by specifically pulling on segments around its posterior curve. Segments of the germ band in this region behave differently from those in its more ventral or dorsal sections. They are mechanically distinct, but more work is needed to explore these segmental differences.

The following chapter includes work published in

Jayasinghe, Aroshan K., **Sarah M. Crews**, David N. Mashburn, and M. Shane Hutson. "Apical Oscillations in Amnioserosa Cells: Basolateral Coupling and Mechanical Autonomy." Biophysical Journal 105 (2013) 255-265.

CHAPTER 3

CARBON DIOXIDE ANESTHETIZATION AS A TOOL TO STUDY DEVELOPMENTAL MECHANICS OF THE AMNIOSEROSA IN *DROSOPHILA* EMBRYOGENESIS

3.1 INTRODUCTION

Drosophila morphogenesis is a dynamic process that involves drastic yet coordinated cell and tissue shape changes. The amnioserosa demonstrates this coordinated movement at the tissue and cellular levels. During germ band extension and germ band retraction, the amnioserosa stretches over the lateral flanks of the embryo and then contracts back onto the dorsal surface of the embryo as the germ band extends and then retracts. Amnioserosa cells change from an isodiametric morphology just before germ band extension, to extremely elongated, back to isodiametric morphology by the end of germ band retraction. In the next stage, dorsal closure, the amnioserosa cells undergo cell shape oscillations. These are clearly observed as sinusoidal variations in each cells apical surface area. These coordinated movements raise the question of: when an individual epithelial cell changes shape, is this process best characterized as viscoelastic or viscoplastic deformation due to forces internal to the deforming cell or forces exerted on that cell by its neighbors?

Previous holographic laser microsurgery experiments that mechanically isolated single amnioserosa cells during dorsal closure showed that the post-ablation behavior of an isolated cell depends on its preablation state (31). Cells that were shrinking when mechanically isolated continued to shrink; however, cells that were ablated while expanding paused before collapsing, and collapsed at an increasingly accelerated rate hinting that the response is not simply a passive one, but rather has significant active contributions.

Here, we use carbon dioxide as a tool to anesthetize embryos in order to separate out the active and passive mechanical contributions. These experiments confirm the mechanical autonomy of amnioserosa cell shape oscillations during dorsal closure.

3.2 MATERIALS AND METHODS

3.2.1 FLY STRAINS AND SAMPLE PREPARATION

Characterization of the carbon dioxide treatment was performed on ubi-E-cadherin *Drosophila melanogaster* embryos (24). Holographic microsurgery experiments were performed on flies expressing *E-Cad:GFP; Sqh:mCherry* (gift from A. Jacinto, Instituto de Medicina Molecular, Lisbon, Portugal).

For holographic microsurgery experiments, embryos were collected and incubated until early-dorsal-closure stage (~24 hours at 15.5°C), dechorionated in a dilute solution of bleach and mounted dorsal-side down on a glass coverslip (26, 32). The mounted samples were then placed in a suitable sample holder for confocal imaging under a layer of halocarbon oil (#27, Sigma-Aldrich, St Louis, MO) and a gas

permeable membrane (YSI, Yellow Spring, OH). Fly embryos were anesthetized by temporarily replacing the air over the sample with water-vapor-saturated CO_2.

3.2.2 LASER ABLATION AND MICROSCOPY

All laser ablation experiments used a laser scanning confocal microscope (LSM 410/Axiovert 135TV, Carl Zeiss, Thornwood, NY) with an attached holographic UV laser ablation system (33). This system simultaneously ablates multiple targeted points by diffracting single pulses from a Q-switched Nd:YAG laser (Minilite II, Continuum, Santa Clara, CA; 5-ns pulse-width, $\lambda = 355$ nm) using a spatial light modulator (PPM X8267, Hamamatsu Photonics K.K., Japan). Tissues were ablated and imaged as close to the apical surface as possible. All microsurgeries were carried out at pulse energies approximately 2-3× threshold to ensure consistent and repeatable ablation. Confocal images were obtained at 4 s/scan, at a resolution of 0.326 µm/pixel, using a 40×, 1.3 NA, oil-immersion objective.

3.2.3 CARBON DIOXIDE ANESTHETIZATION

CO_2 anesthesia is administered by flowing carbon dioxide over the sample. A hole is punctured through a petri dish lid. CO_2 is bubbled through water to water-saturate the gas which then flows through tubing onto the sample as shown in Figure 16.

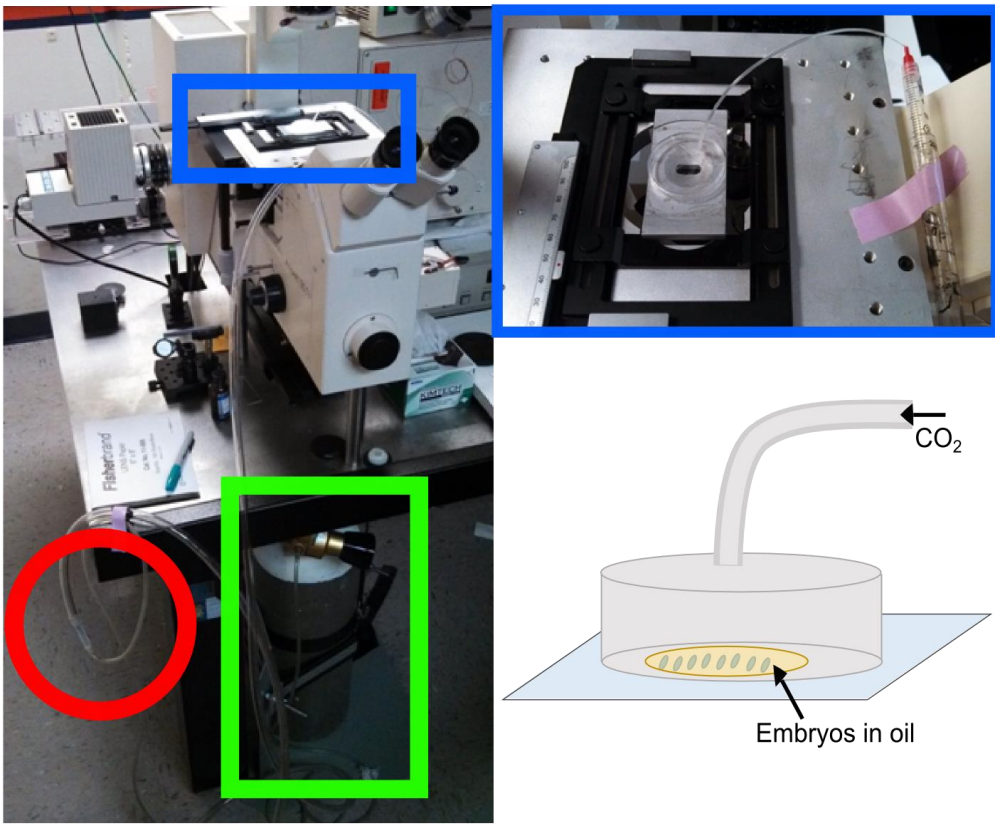

Figure 16. Carbon dioxide anesthetization setup. CO_2 (tank circled in green) bubbles through tubing filled with water (circled in red). The water saturated carbon dioxide then flows over the sample (boxed in blue). An enlarged image of the sample is shown top right and a schematic of the sample is shown bottom right.

3.2.4 IMAGE PROCESSING AND ANALYSIS

We used ImageJ (NIH, Bethesda, MD) software for basic image processing tasks. To measure the areas and volumes of cells, we used Seedwater Segmenter (29), a custom watershed-based segmentation software. 2.7 Segmentation

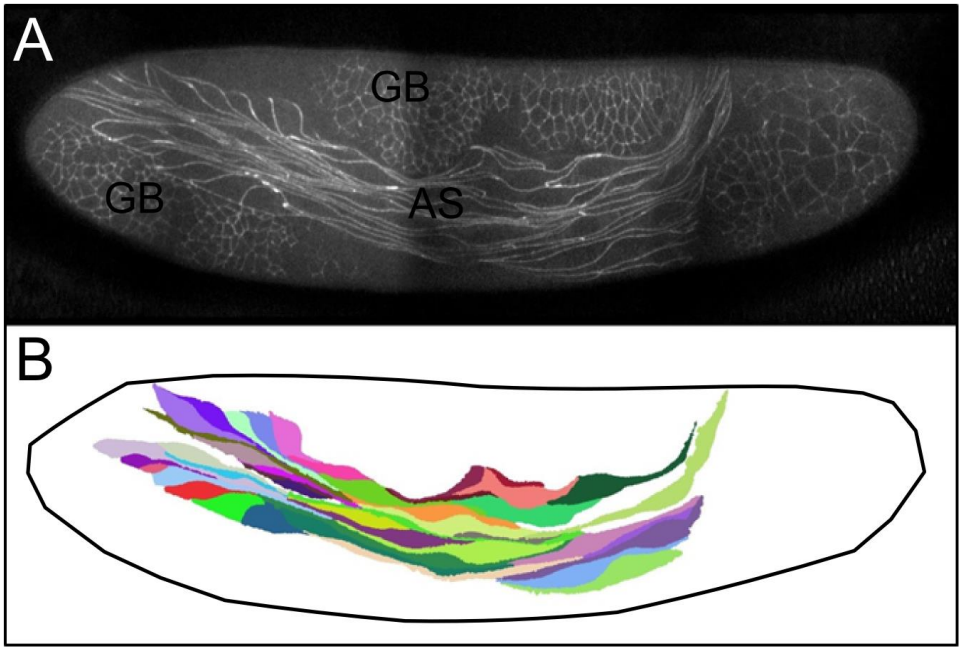

Figure 17. Segmentation example. (A) Confocal image of embryo in early germ band retraction. (B) Segmented image of the amnioserosa from image in (A).

In order to quantify morphological information such as the area, perimeter, or aspect ratio of individual cells, it is necessary to segment the collected confocal images. Here, we used SeedWater Segmenter, a watershed-based algorithm that allows for automated segmentation along with user modifications. This program also allows for single cells to be tracked through a timelapse image set (29). Figure 17 shows an example of a confocal image and the corresponding segmented image.

3.3 RESULTS

3.3.1 ANESTHETIZATION

Anesthetization of embryos is performed by replacing the air above the embryos with carbon dioxide (CO_2). After just a few minutes of CO_2 exposure, embryos halt active movements. This is confirmed by monitoring the pulsations of amnioserosa cells

apical surface area during dorsal closure (Fig 18). Under ambient conditions, the amnioserosa cells pulse with a period of approximately 240 seconds or 4 minutes (34–36); after the application of CO_2, the cells become static. After the source of CO_2 is removed and oxygen is again able to reach the embryos, the pulsations resume and embryos are able to complete development. To make sure that this behavior was not a response specific to CO_2 exposure, we also exposed embryos to argon gas using an identical protocol. Similar cell behavior was seen, showing that this anesthetization is a result of oxygen depletion not just a reaction specific to CO_2 exposure.

This anesthetization procedure does not significantly affect embryo viability. E-cad-GFP embryos were dechorionated and mounted on a slide, then subjected to one hour of carbon dioxide treatment during germ band retraction or dorsal closure. CO_2 was removed, and the embryos were then left to develop at room temperature. Of the 50 embryos tested, 38% hatched out as larva compared to 44% hatching for control embryos (N=50). These distributions are not significantly different ($p=0.68$); from this we can conclude that CO_2 is a safe anesthetization method, at least for embryos in mid to late embryogenesis.

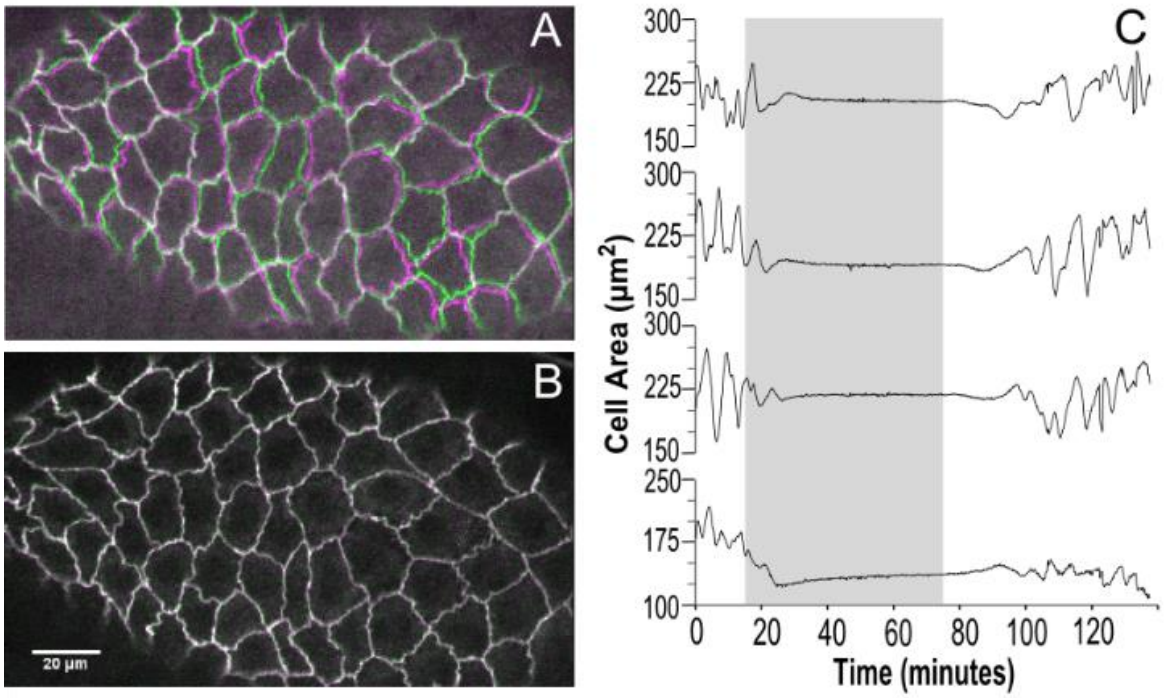

Figure 18. Cell pulsations cease after CO_2 is applied. Overlay of images taken at times (A) before CO_2 is applied at t=1 and t=33 minutes and (B) while embryo was anesthetized at t=60 and t=62 minutes (C) Plots of apical area versus time for four different amnioserosa cells. Pulsations cease within 10 minutes of CO_2 application and resume 15 minutes after CO_2 is removed.

3.3.2 CELL ISOLATION USING HOLOGRAPHIC LASER MICROSURGERY

To investigate the role of active responses, we blanketed fly embryos with CO_2 gas and conducted cell isolation experiments. Our protocol for ablation targets all neighbors of the cell to be isolated with ablation near the middle of each neighbor-neighbor interface—like targeting spokes emanating from the cell to be isolated. These interfaces often move during the targeting process, so we ablate two closely spaced points for each interface to maximize the chance for a clean and complete cut (33). The ablated locations are visible in Fig. 19, B-E, as the static dark spots resulting from puncture wounds in the embryo's encasing vitelline membrane. Leakage through these holes is prevented by a glue layer between the membrane and coverslip (26). Within the

embryo, each laser wound extends clean through the ~6-µm-thick epithelium (26). We specifically target cell-cell interfaces because previous work has shown that such wounds quickly and effectively destroy all mechanical integrity in the two targeted cells (37).

When CO_2 is applied during early dorsal closure, amnioserosa pulsations and their associated dynamic myosin accumulations cease within 4 min (Figure 19F), but residual tissue motion continues a few minutes longer, presumably until the cells reach a mechanical equilibrium under passive tension. We chose to wait ~15 min after starting CO_2 flow before mechanically isolating a single cell.

As shown in Fig. 19, the apical area of the cell to be isolated stabilizes during the CO_2 exposure, and then undergoes an immediate, but slight, post ablation recoil (losing <12% of its area). During the next 500 s, as the flow of CO_2 continues, the isolated cell retains its shape and area. The outer boundary of the wound opens slowly, but similarly retains its ragged shape. There are no changes in the accumulation of myosin, neither apical nor basal. We then stopped the flow of CO_2 at 500 s after ablation and observed the longer-term resumption of an active response. Only ~900 s later does the wound start to significantly reshape (Figure 19D). This reshaping is accompanied by a weak accumulation of myosin at the wound margin. By 2000 s after ablation (1500 s after CO_2 removal), wound healing is underway, but the isolated cell retains ~76% of its preablation apical area (Figure 19F). Approximately 2500 s after ablation, there finally appears to be a strong contraction of the isolated cell's apical surface. At this point, the isolated cell's edges are significantly dimmer than the rest of the tissue—possibly due to the degradation of fluorescently labeled cadherin

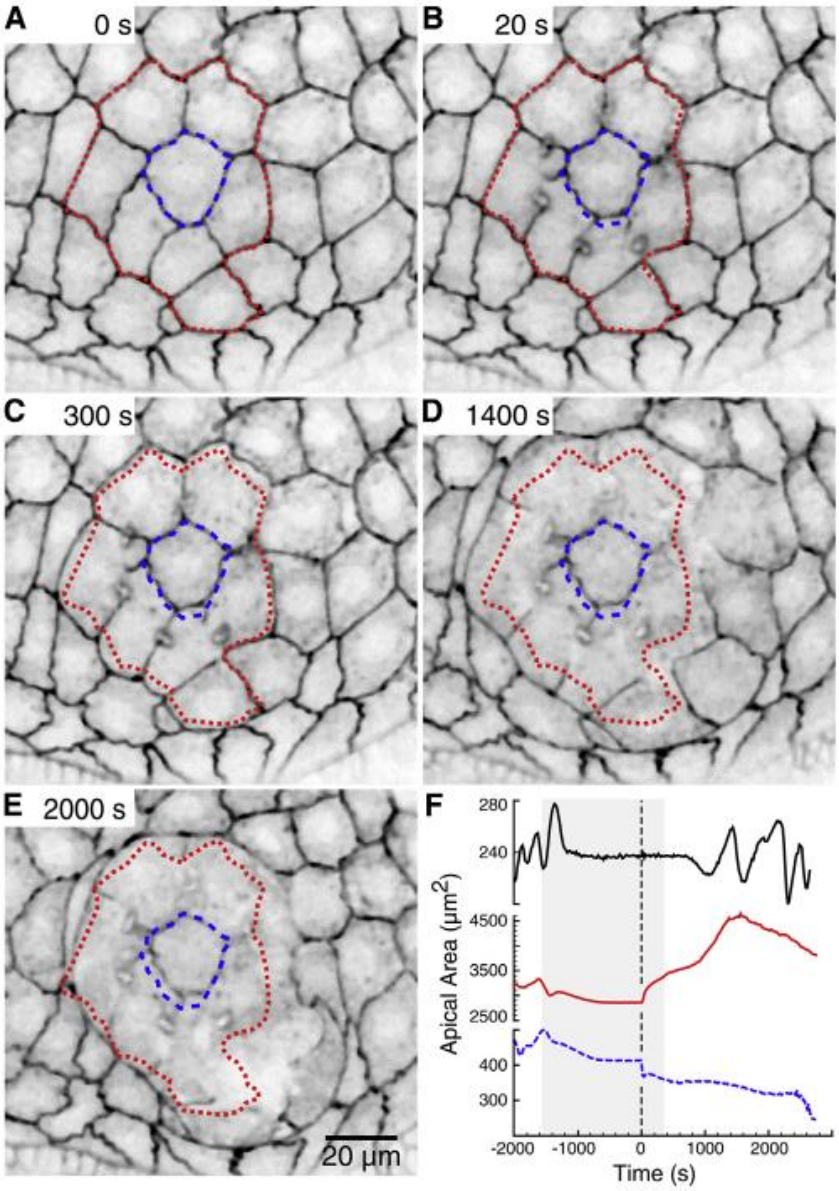

Figure 19. Cell isolation experiment in a CO2-anesthetized embryo**.** (A–E) Pre- and postablation confocal images (inverted grayscale) showing slow retraction of the wound and almost no contraction of the isolated cell. Each panel is labeled at upperleft with the elapsed time after ablation.Overlays denote preablation shapes of the isolated cell (blue dashed) and the outer boundary of the wound (red dotted). A common scale bar is shown in panel E. (F) Comparison of cell shape dynamics for the total area inside the outer wound margins (red) and the apical area of the isolated cell (blue dashed). To place these dynamics in the context of when active responses resume, the uppermost curve shows area changes for a cell in a different embryo exposed to CO_2 for the same length of time, but not ablated (black). (Shaded region) Duration of CO_2 exposure.

junctions—which makes quantification of cell area difficult. We were also unable to observe any significant myosin accumulation near the apical surface of the contracting isolated cell. Nonetheless, it is clear that passive relaxation of elastic strain only accounts for a few percent of the isolated cell's contraction; the large remainder requires an active response.

3.4 DISCUSSION

Here, we show that carbon dioxide anesthetization, a common technique for *Drosophila* adults and larvae is a useful technique for studying embryogenesis. The utility of this technique for separating out active and passive mechanical contributions in morphogenesis is demonstrated by cell-isolation experiments during dorsal closure. The ability of an isolated cell to maintain its area after isolation while under anesthesia proves that the collapse of an isolated cell is driven not by passive elastic relaxation, but is rather driven by active processes and corroborates the results of the same experiments performed on non-anesthetized embryos. This shows the mechanical autonomy of amnioserosa cell pulsations. These results are important to inform computational models of epithelia, which previously modeled oscillations as high elastic strain deformations. These results mark a substantial advance in our understanding of epithelial mechanics at the cellular level.

CHAPTER 4

PARTICLE TRACKING MICRORHEOLOGY IN AMNIOSEROSA DURING GERM BAND RETRACTION

4.1 INTRODUCTION

The deformability of a tissue is regulated by its viscoelastic properties. Processes like amnioserosa cell shortening as seen in germ band retraction or like the contractile pulsations in dorsal closure are examples of such deformations. Knowledge of these viscoelastic parameters is also important for interpreting strain measurements and for implementation of computational models (26, 38). Microrheology, or the study of viscoelasticity of materials at the microscopic scale, includes a variety of techniques to probe these parameters, for example, atomic force microscopy or micropipette suction (39–42). Unfortunately these techniques, are not well suited for *in vivo* studies where the tissues are not directly accessible to external probes. Here we use a method of passive microrheology—particle tracking microrheology—to measure the viscoelastic parameters of the amnioserosa during a stage of significant cell shape changes—germ band retraction (43–45).

Germ band retraction is a 2-3 hour morphogenetic process which begins approximately 7 hours post fertilization. At the beginning of germ band retraction, the amnioserosa is in a saddle shape tissue stretching over the lateral and dorsal surfaces of the embryo; the adjacent germ band extends from the ventral surface around the posterior end of the embryo onto the dorsal surface. The amnioserosa cells are extremely elongated to a mean aspect ratio (defined by length divided by width of cell)

of approximately 11 (10). As the germ band retracts back around the posterior end of the embryo, the amnioserosa tissue rounds and the cells become more isodiametric.

All of this motion requires the rearrangement of the cell cytoskeletons, however; it can be difficult to discern active deformations from passive ones. Here we use carbon dioxide to halt the active movements in the embryo to be able to measure the intrinsic viscoelastic properties of the tissue. Using this anesthetization technique paired with particle tracking microrheology, we show that the viscosity of amnioserosa cells decreases from early to late germ band retraction and the weak anisotropy that is present in early germ band retraction disappears as retraction progresses.

4.2 MATERIALS AND METHODS

4.2.1 MICROINJECTIONS

Fluorescent beads (100nm diameter, Molecular Probes) suspended in water were PEGylated as described in (44, 46) and injected into embryos using pulled capillary needles. Injections were performed on dechorionated embryos before cellularization (Bownes stage 5, 130 minutes post fertilization), and thus before membranes form around the nuclei at the periphery of the embryo. This way, beads can be incorporated into cells during cellularization. The success of microinjections is highly dependent on the size and rigidity of the needle used. The needles used in the microinjections were pulled using a Flaming Brown Micropipette Puller (Sutter Instruments, Model P-80/PC). Needles were then trimmed with a scalpel and beveled such that the outer diameter of the needle is approximately 7-8 microns (Figure 20).

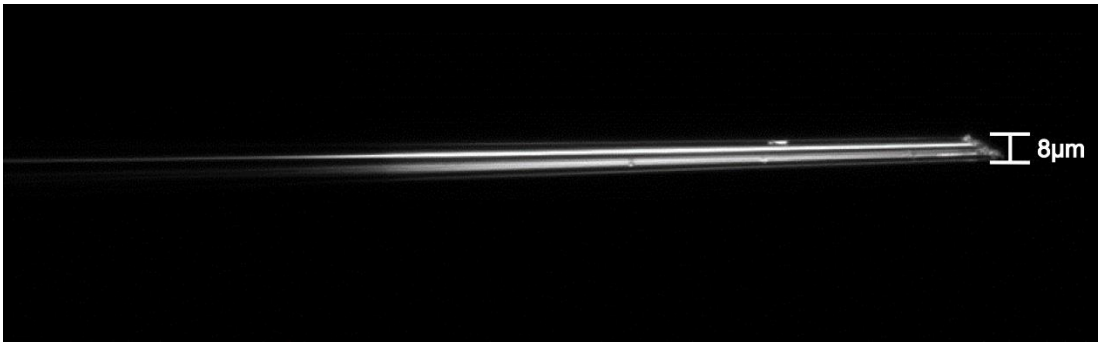

Figure 20. Needle for microinjections. Microcapillary tube that has been pulled and beveled such that the outer diameter of the needle tip is approximately 8µm.

The injections were performed using a microinjector (Narishige, IM 300 Microinjector). Embryos were injected near the micropyle at the anterior portion of the embryo (Figure 21). Care must be taken to not insert the needle too far into the embryo (only about 1/3 of the length of the embryo), and for optimal survival, leakage from the embryo should be minimized. After injections, the embryos were stored in an incubator at 15º Celsius overnight before imaging.

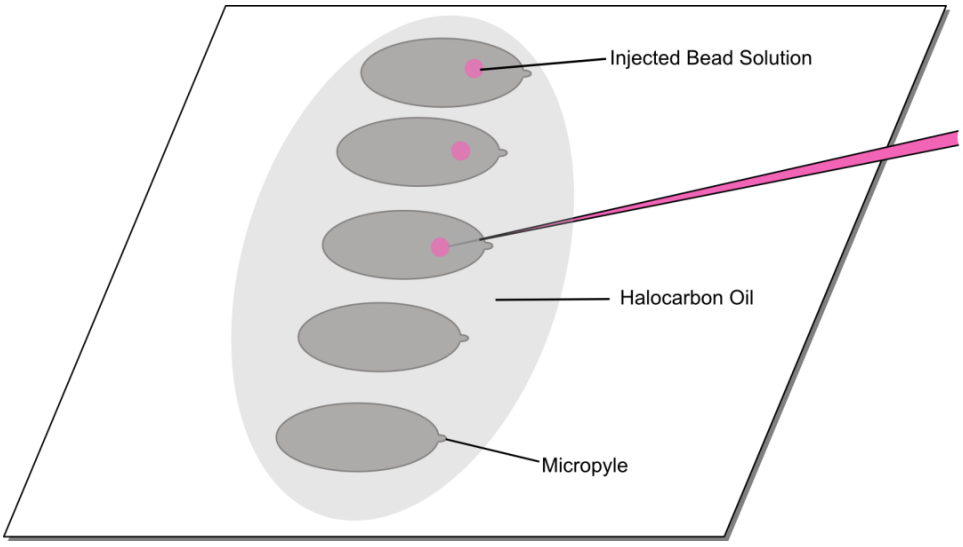

Figure 21. Microinjection set up. Embryos are mounted on a coverglass and covered with halocarbon oil. Embryos are injected with bead solution through a sharp needle inserted on the anterior portion of the embryo near the micropyle.

4.2.2 IMAGE PROCESSING AND ANALYSIS

ImageJ (NIH, Bethesda, MD) software was used for image processing. Particle tracking was performed using the Trackmate plugin of ImageJ (47). Calculation of mean square displacement and viscosity were performed using Mathematica.

4.2.3 IMAGING

Time lapse images of the beads inside cells were captured on a Nikon spinning disk microscope at 160 ms per frame.

4.2.3 DATA FITTING

The x and y positions of the beads were tracked through time using the ImageJ plugin TrackMate (48). The x and y positions were rotated such that the x-axis was along the long axis of the amnioserosa cells in each embryo. From this, the mean square displacement (MSD) as a function of time lag, τ, for each bead trajectory was calculated as below:

$$MSD_x(\tau) = \langle \big(x(t+\tau) - x(t)\big)^2 \rangle \quad (1)$$

$$MSD_y(\tau) = \langle \big(y(t+\tau) - y(t)\big)^2 \rangle \quad (2)$$

$$MSD_r(\tau) = MSD_x(\tau) + MSD_y(\tau) \quad (3)$$

$$= \langle \big(x(t+\tau) - x(t)\big)^2 + \big(y(t+\tau) - y(t)\big)^2 \rangle$$

The mean square displacements for all beads were averaged together before being fit to an anomalous diffusion model.

Non-disrupted diffusion of a particle in a homogenous medium is linear with time and proportional to a diffusion constant, D:

$$MSD(\tau) = 2^n D\tau, \quad (4)$$

where n is the number of degrees of freedom measured. In biological systems, however, the diffusive medium is often heterogeneous. In the case of active cellular transport, a particle may experience superdiffusion, or in the case where there are obstructions present, such as cytoskeletal components or other vesicles, a particle may exhibit subdiffusion (Figure 22). In these cases, displacement from diffusion is not linear with time, but instead proportional to some fractional exponent of time.

$$MSD(\tau) = 2^n D\tau^{\alpha} \quad (5)$$

Knowledge of the value of the anomalous exponent, α, gives insight into how obstructed movement is within the medium. Superdiffusion will fit to the form where α>1. In the special case of ballistic motion, α is equal to 2. For subdiffusion, α will be less than 1 (49).

The Stokes-Einstein equation relates the diffusion constant, D, found from fitting the mean square displacement curve to the viscosity, η, for spherical objects undergoing Brownian motion.

$$D = \frac{kT}{6\pi\eta r}, \quad (6)$$

where k is the Boltzmann constant, T is temperature, and r is the radius of the spherical object. For the bead experiments discussed in this paper, r = 50 nm.

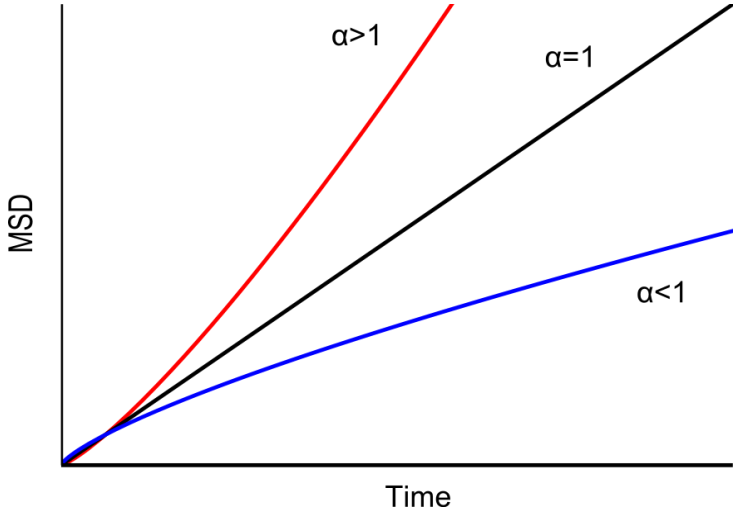

Figure 22. Anomalous diffusion model. Super diffusion is shown in red and subdiffusion is shown in blue.

4.3 RESULTS

For particle tracking microrheology, we first had to get beads into the amnioserosa cells. Beads were injected into embryos within the first two hours post-fertilization before embryos entered cellularization. The beads could then be incorporated into cells as cell membranes form around cell nuclei. Figure 23A shows beads inside amnioserosa cells. Timelapse images of the beads were taken at 160 ms/frame, and the two-dimensional position of each bead was tracked through time. Figure 23B shows several sample bead trajectories. The mean square displacement was calculated for each bead. All MSDs were averaged for trajectories collected during

early germ band retraction and also for late germ band retraction. The average MSDs are represented by the dotted lines in Figure 24A-B.

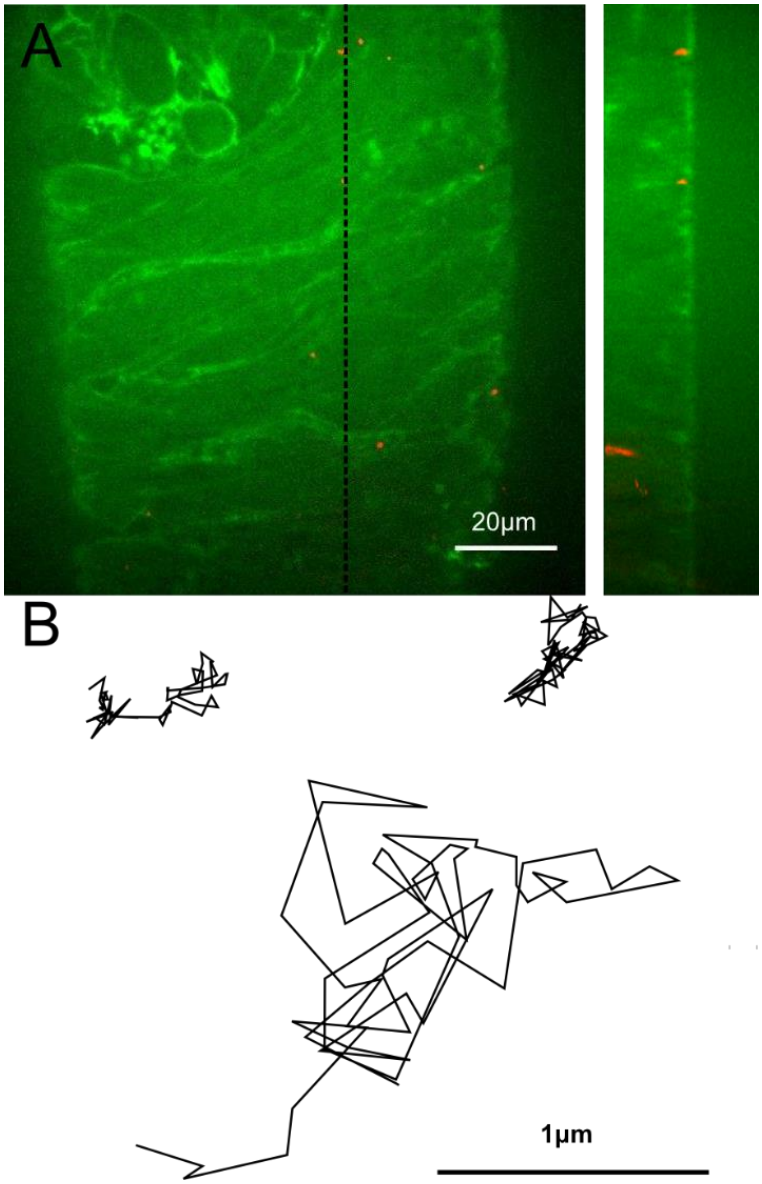

Figure 23. Fluorescent bead motion is tracked inside cells. (A) Images showing and yz (right) planes showing that beads are in fact inside amnioserosa cells. (B) Sample tracks of three beads.

The trajectories in these experiments actually appear to represent superdiffusive behavior, with an increasing slope at longer time delays. This could be from active transport within the cells, or from the flow of beads and cytoplasm as cells move. To circumvent this problem, we anesthetized the same embryos with carbon dioxide and tracked the subsequent Brownian motion of the beads. The average MSDs are shown with the solid lines in Figure 24A-B. The movement of the beads under carbon dioxide appear to represent subdiffusive behavior. This comparison demonstrates the effectiveness and necessity of anesthetization for microrheological measurements.

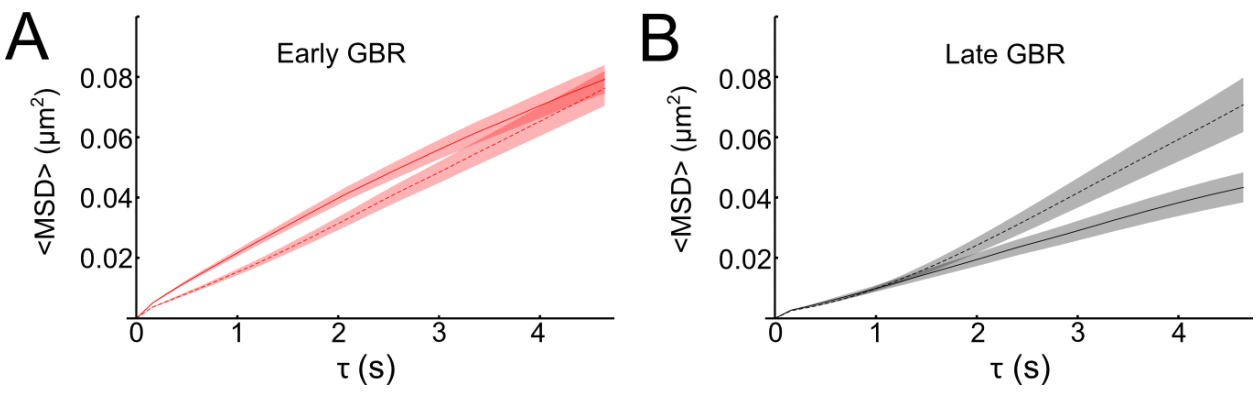

Figure 24. <MSD> before (dashed line) and during (solid line) carbon dioxide anesthetization for (A) early germ band retraction and (B) late germ band retraction. Shaded regions represent standard error of the mean.

Comparisons of the average MSDs under CO_2 anesthetization are shown in Figure 25A for early and late germ band retraction. Each <MSD> was fitted to an anomalous diffusion model, allowing for estimation of the viscosity and anomalous diffusion exponent for each stage. The viscosity of amnioserosa cells in early germ band retraction is approximately 17 Poise and drops to approximately 8 Poise by late germ band retraction. The anomalous exponent also drops from 0.96 to 0.84. The

values for the viscosity and anomalous exponent are found in Table 2. Note that the viscosity during late germ band retraction is half of what it is in early germ band retraction, while the anomalous exponent only differs by approximately 10%. We also looked at the diffusion of beads in the perivitelline fluid, which is between the vitelline membrane and the epithelium of the embryo. These beads exhibited nearly pure diffusion ($\alpha = 0.960 \pm 0.022$), giving an estimated viscosity of the fluid of 1.14 ± 0.008 Poise, approximately 100 times more viscous than water.

	Viscosity (Poise)	**Anomalous Exponent**
Early GBR	17.4 ± 0.1	0.957 ± 0.006
x-diffusion	17.1 ± 0.2	1.042 ± 0.010
y-diffusion	17.6 ± 0.2	0.857 ± 0.008
Late GBR	7.92 ± 0.04	0.835 ± 0.004
x-diffusion	8.08 ± 0.03	0.816 ± 0.003
y-diffusion	7.77 ± 0.05	0.852 ± 0.005
Perivitelline Fluid	1.14 ± 0.01	0.960 ± 0.022

Table 2: Anomalous Diffusion Fit Parameters

We then looked to see if there was anisotropy in bead diffusion of the beads. We separately considered diffusion in two orthogonal directions (x and y) such that the x-direction was along the long axis of amnioserosa (Figure 25B). In early germ band retraction, particles diffuse slightly faster along the direction of cell elongation (x) (Figure 25C). This anisotropy disappears by late germ band retraction (Figure 25D). The change may be attributed to reorganization of the cytoskeleton as cells shift from an extremely elongated morphology to more isodiametric shapes.

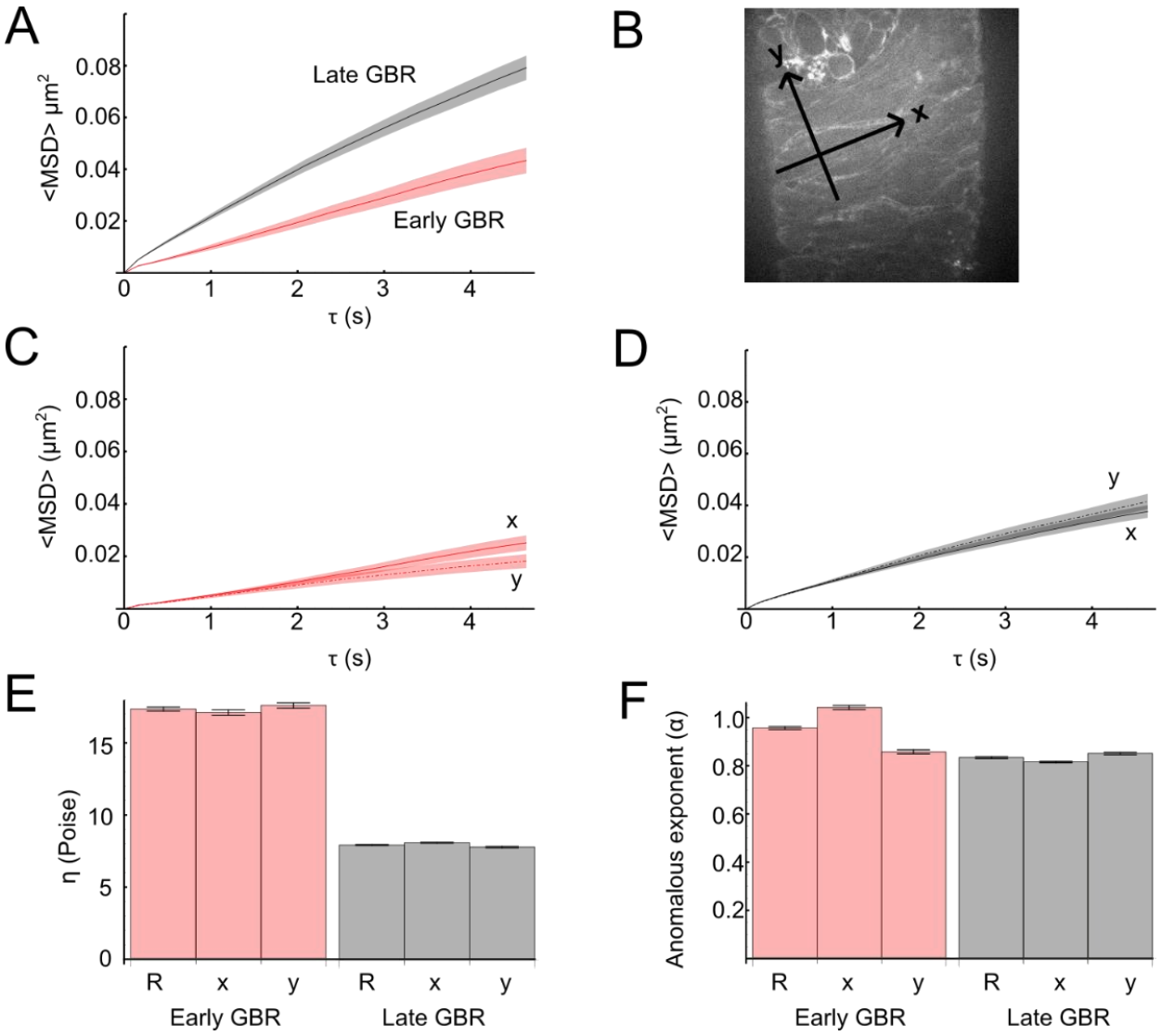

Figure 25. <MSD> comparison for early (red) and late (gray) germ band retraction: (A) two dimensional <MSD>; (B) coordinate system; diffusion along x-axis and y-axis for (C) early germ band retraction and (D) late germ band retraction. Shaded regions represent standard error of the mean. Viscosity (E) and anomalous diffusion exponent values (F) were estimated by fitting <MSD> anomalous diffusion model. Error bars represent standard error.

4.4 DISCUSSION

Here we demonstrate the use of particle tracking microrheology to probe the viscosity of the amnioserosa during germ band retraction. This is a novel finding as microrheological measurements inside *Drosophila* embryos are difficult due to the inability

to directly access their cells *in vivo*. Active fluctuations are halted using carbon dioxide anesthetization to allow measurement of the passive viscoelastic parameters of the cells. Viscosity estimates ranged from approximately 8 to 17 Poise in the amnioserosa during germ band retraction. This is on the same order of magnitude for viscosities reported in sea urchin embryos (η~10-100 Poise)(50), *C. elegan* embryos (η~10 Poise)(44), and mouse embryonic fibroblasts (η~18 Poise)(51).

Interestingly, this mechanical property is not constant. As the germ band retracts, the viscosity and anomalous diffusion exponent decrease. There is also anisotropy present in early germ band retraction. When the amnioserosa cells are extremely elongated during early germ band retraction, particles are more free to move along the axis of cell elongation. As the germ band retracts and the cells become more isodiametric, this anisotropy diminishes. These results demonstrate how dynamic the viscoelastic properties of living tissues can be. The viscosity of the amnioserosa cells decrease by a factor of 2 within the two hours of germ band retraction, suggesting that not only does the viscosity regulate how easily cells can deform, but the shape of a cell may also regulate this viscosity.

The work in the following chapter was performed in collaboration with W. Tyler McCleery

CHAPTER 5

HEAT SHOCK-INDUCED EPITHELIAL HOLES DURING *DROSOPHILA MELANOGASTER* EMBRYOGENESIS

5.1 INTRODUCTION

Non-specific environmental stress is known to cause developmental defects in embryogenesis. For example, maternal exposure to alcohol during pregnancy leads to developmental delays and growth deficiency in the fetus (52). Similarly, hyperthermia during development has been associated with defects of the central nervous system including neural tube defects (53–56). The type and severity of defects is strongly dependent on the stage at which the environmental insult is introduced (20, 57). Here, we investigate disrupted development in *Drosophila melanogaster*, specifically of the amnioserosa and germ band, after embryos are exposed to a non-specific heat shock administered at the start of gastrulation.

The amnioserosa and germ band are monolayered epithelial tissues in *Drosophila* embryogenesis that move in a coordinated fashion for much embryonic development. Immediately following gastrulation, the embryo enters into germ band extension (Bownes stage 8). Here, the germ band lies on the ventral side of the embryo and actively extends around the posterior end of the embryo. Meanwhile, the amnioserosa cells elongate over the dorsal surface of the embryo and onto its lateral flanks. After extension, the germ band will then retract back around the posterior end of

the embryo as the amnioserosa cells round up and move back to the dorsal surface. Finally, the embryo enters into a stage called dorsal closure. Previously, we have shown that the amnioserosa is mechanically essential for the completion of germ band retraction and assists in dorsal closure before undergoing apoptosis. Specifically, germ band retraction fails in the absence of an intact amnioserosa as demonstrated by destruction of the amnioserosa with laser microsurgery (14). This finding is validated by the *u-shaped* group of mutants in which the amnioserosa is severely deformed or altogether absent (13), leading to defects in germ band retraction. Interestingly, hours after heat shock, embryos exhibit a range of defects including problems completing germ band retraction (20). We thus hypothesize that heat shock at gastrulation causes a loss of mechanical integrity of the amnioserosa.

Here, we find that this loss of integrity of the amnioserosa is due to large holes that open in the tissue. These holes are acellular and appear to open along cell-cell interfaces. We investigate three possible causes for hole initiation and track its subsequent effects on development: extra mechanical stress that rips the amnioserosa open; inadequate adhesion along cell edges by compromised adherens junctions; or premature apoptosis in the amnioserosa. We find evidence that a misregulation in timing between the amnioserosa and the germ band causes the amnioserosa to mature significantly faster than the germ band, and therefore undergo premature apoptosis. The amnioserosa cells become stiffer, increase adherens expression, and stochastically present delamination events similar to those events found normally in dorsal closure, all while the germ band is extending and retracting. Based on these results, we present a model: heat shock decouples the coordinated timing of the amnioserosa and the germ

band. This heterochronicity leads to a premature loss in the mechanical integrity of the amnioserosa and ultimately failure of the embryo to complete development.

5.2 MATERIALS AND METHODS

5.2.1 FLY STRAINS

We used several fluorescently labeled strains of *Drosophila melanogaster*: *ubi-DE-Cad-GFP* (24) (Drosophila Genetic Research Center, Kyoto, Japan), which ubiquitously expresses E-Cadherin–GFP to label epithelial cell junctions; sGMCA-3.1 (3rd chromosome insertion; gift from DP Kiehart, (25)) to visualize actin filaments; E-Cad:GFP; Sqh:mCherry (gift from A. Jacinto, Instituto de Medicina Molecular, Lisbon, Portugal) for visualization of cell edges and myosin activity; Gap43 (gift from Adam Martin, Massachusetts Institute of Technology) to label membranes; UAS-Apoliner (58) (Bloomington Stock Center) as a fluorescent sensor of apoptosis-associated caspase activity.

5.2.2 SAMPLE PREPARATION FOR LIVE IMAGING

Embryos were collected on grape agar plates with yeast paste for one hour collections. Embryos were left at room temperature to develop for two hours. They were then washed with 50% bleach solution to remove the chorion, and mounted on a coverslip using embryo glue. Mounted embryos were surrounded with wet strips of Whatman filterpaper, and covered with an oxygen permeable membrane (YSI, Yellow Spring, OH) to prevent dehydration while allowing sufficient oxygen exchange.

5.2.3 HEAT SHOCK

The standard protocol for mounting embryos requires covering the embryos with halocarbon oil to prevent desiccation; however, we found that embryos covered in oil did not survive a 30-minute heat shock. Therefore, we had to develop an oil-free mounting method. For the heat shock experiments, embryos were mounted on a cover glass and surrounded by water-saturated filter paper. All of this was sealed with an oxygen permeable membrane to prevent dehydration.

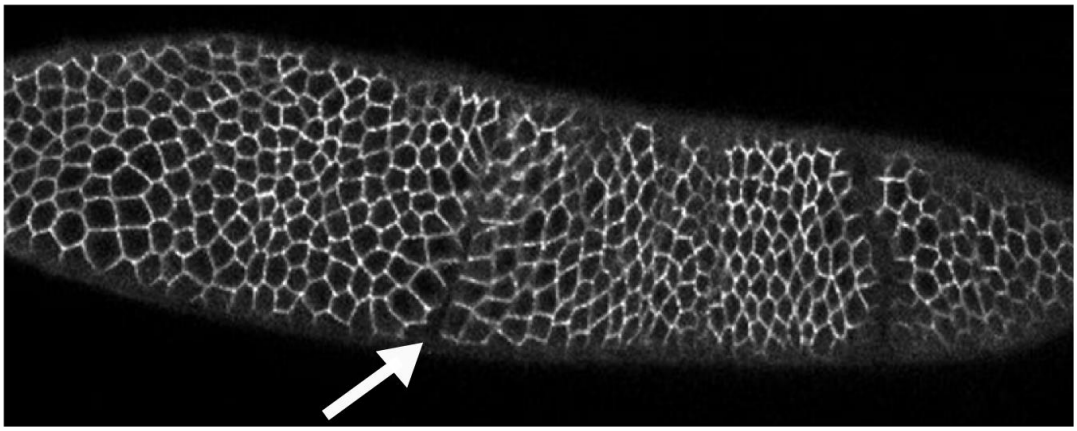

Figure 26. Cephalic furrow marks start of gastrulation. Heat shock is administered just after the formation of the cephalic furrow (white arrow)

The long-term effects of heat shock are dependent upon the stage and severity of the shock (20). The heat shock experiments described here required administration of a heat shock at the beginning of gastrulation (Bownes stage 6), a stage which only lasts approximately 15 minutes. Embryos were therefore closely monitored through the eyepieces of a Zeiss LSM410 inverted microscope with a 40×, 1.3 NA oil-immersion objective under bright field illumination. As soon as the cephalic furrow of one or multiple embryos on a slide became apparent (Figure 26), the slide was moved to float

on a 38 ºC water bath. After 30 minutes, the slide of embryos was removed and the embryos were left to recover at room temperature until fixation or imaging.

5.2.4 MICROSCOPY AND IMAGE ANALYSIS

Fluorescent imaging was performed on either a laser scanning confocal microscope (LSM 410/Axiovert 135TV; Carl Zeiss, Thornwood, NY) with a 40x 1.3NA oil-immersion objective at .649 μm/pixel or a spinning disk confocal microscope (Eclipse Ti; Nikon Instruments, Melville, NY, and Quorum WaveFX-X1, Ontario, Canada) using a 40x 1.3NA oil-immersion objective at .22 μm/pixel.

For measurements of cell morphology, we segmented images of E-cad-GFP amnioserosa cells using a watershed-based segmentation software, Seedwater Segmenter (29). From the segmentation we extracted information on area, perimeter, and aspect ratio.

5.2.5 DAPI AND IMMUNOSTAINS

Embryos were fixed in 1:1 heptane and 16% formaldehyde solution for 4 minutes. The formaldehyde and heptane was removed, and the embryos were then devitillinized in a 1:1 methanol and heptane solution by vigorous shaking for 30 seconds. Embryos were stored overnight in methanol at 4°C. Embryos were then rehydrated in PBTA (mixture of phosphate buffered saline (PBS), bovine serum albumin, sodium azide,and Triton-X 100, (59)), on a rotator for 15 minutes. To look at hole morphology, embryos were stained with primary antibodies for α-spectrin (3A9 Alpha-Spectrin antibody solution) and β-integrin (CF.6G11 Integrin antibody solution)(Developmental Studies Hybridoma Bank, University of Iowa), and then with

secondary antibodies AlexaFluor 568 Goat Anti-Mouse IgG2b and AlexaFluor 488 donkey anti-mouse (Molecular Probes, Life Technologies, Grand Island, NY). To look at E-cadherin expression, embryos were stained with primary antibody DCAD2 (Developmental Studies Hybridoma Bank, Univeristy of Iowa) and secondary antibody FITC (Jackson ImmunoResearch, West Grove, PA).

Embryos were washed in PBTA before adding 100X DAPI solution (59) for five minutes. Embryos were then washed extensively in PBTA followed by several washes in PBS. Embryos were mounted in glycerol-based mounting medium (59) for imaging.

5.2.6 LASER HOLE DRILLING AND ANALYSIS

Laser hole drilling was conducted using the above mentioned laser scanning confocal microscope and single pulses from the 3rd harmonic (355 nm) of a Q-switched Nd:YAG laser (5 ns pulsewidth, Continuum Minilite II, Santa Clara, CA). Images were collected at zoom 4 with at .649μm/pixel at a rate of 1 s per frame. Post-ablation radial strains were estimated from the deformation fields around laser-induced holes as calculated using bUnwarpJ (60). These deformation fields were applied to circles of radii 8 μm, 16 μm, and 24 μm centered on the wounds. The areas of these deformed circles were used to calculate the radial strain, ε_r, of the tissue after ablation given by

$$\varepsilon_r(t) = \frac{\sqrt{A(t)} - \sqrt{A(t_0)}}{\sqrt{A(t_0)}} \tag{14}$$

where A is the area of the circles centered on the ablation points.

5.3 RESULTS

5.3.1 HEAT-SHOCK-INDUCED HOLES IN THE AMNIOSEROSA

To investigate the cause of heat-shock-induced developmental defects, *Drosophila* embryos were exposed to a 30 minute, 38°C heat shock just as the cephalic furrow formed at the onset of gastrulation. All stages of embryonic development were analyzed after heat shock using *in vivo*, time-lapse confocal imaging of GFP-E-Cadherin tagged flies. The embryos appeared to recover from heat shock and proceeded through development normally, albeit at a slower rate. Surprisingly, hours after the shock an extra-embryonic epithelial tissue, the amnioserosa, often developed holes. The formation and growth of one such hole is shown in Figure 27A. Notably, nine hours after gastrulation the hole grew to a diameter of 150 μm – the full width of the amnioserosa tissue. Similar holes were found in all five of the strains we looked at with live imaging.

Phototoxicity is also sufficient to cause holes in the amnioserosa (data not shown). To avoid effects of photoxicity, we also performed a second set of experiments where the heat-shocked embryos were not imaged until 7-8 hours post-gastrulation. These embryos also exhibited holes in the amnioserosa. All of these holes opened in the dorsal or dorso-lateral portion of the amnioserosa, but not along the lateral flank; no holes were observed in the germband. Here, we present a series of experiments to

elucidate the effects of these holes on development and possible causes that lead to hole initiation.

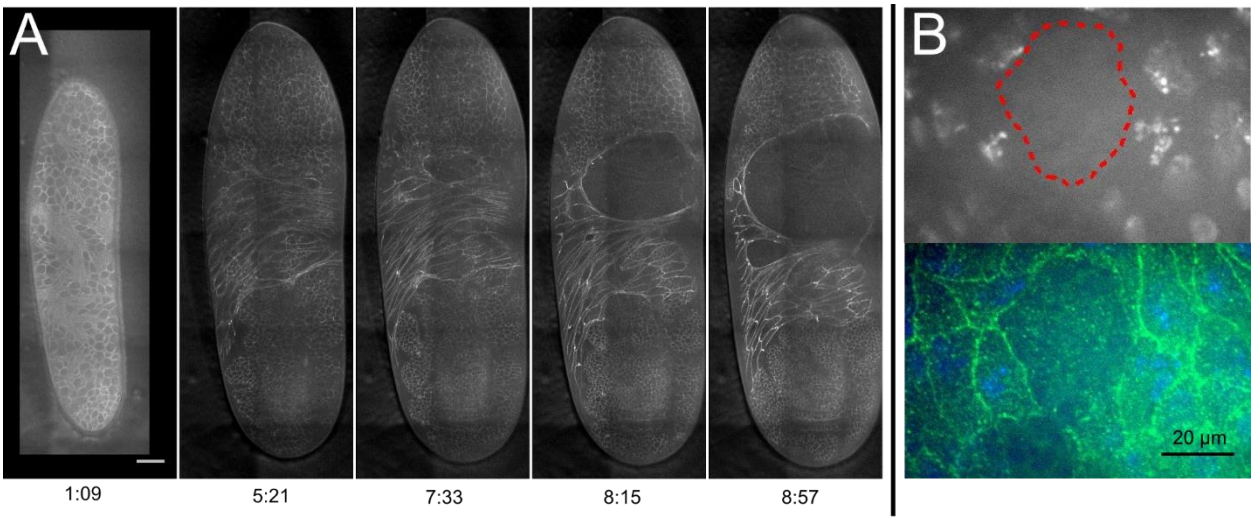

C

		Head Defect		Seg. Defect		Failure GBE		Failure GBR		Failure DC	
		TRUE	FALSE	TRUE	FALSE	TRUE	FALSE	TRUE	FALSE	TRUE	FALSE
Hole in AS	TRUE	21	7	2	6	4	27	12	14	17	9
	FALSE	7	11	2	14	-	18	2	16	2	16
p-Values		0.016*		0.407		0.148		0.015*		<0.001*	

Figure 27. Heat-shock-induced holes in the amnioserosa. (A) Timelapse image of a hole opening. Time is in hours post-gastrulation. Dorsal side is shown with anterior up in all images. (B) DAPI nuclear staining (top) around a hole (red outline) and overlay of DAPI with α-Spectrin membrane marker (bottom) indicate there is no nucleus or nuclear fragments inside the hole. (C) Correlation table of holes to developmental defects. Statistically significant correlations ($p < 0.05$) between holes and defects are denoted by an asterisk (*). See text for explanation of defects: Seg., segmentation; GBE, germ band extension; GBR, germ band retraction; DC, dorsal closure.

5.3.2 HOLES CORRELATE TO DEVELOPMENTAL DEFECTS

To determine the impact of the holes on development, we catalogued the variety and prevalence of these holes along with other developmental defects. We heat shocked 53 E-Cadherin-GFP embryos and 31 Moesin-GFP embryos and imaged each embryo only twice to avoid phototoxic effects: once 7-8 hours after gastrulation and again approximately 20 hours after gastrulation. These embryos were scored for several

defects: failure of germ band extension, failure of germ band retraction, failure of dorsal closure, head defects, segmentation defects, and holes. The prevalence of the defects and holes in both fluorescently-labeled strains are compared to values reported by Eberlein (1986) (20) in Table 3. Although the presence of holes in the cuticle has been mentioned previously in the literature, we believe these holes, appearing within the amnioserosa tissue rather than the cuticle, are unique and thus a novel discovery. Previous reports of holes in the cuticle following heat shock or in mutants are likely to be the result of germ band retraction and dorsal closure defects that prevented cuticle-depositing tissues from completely covering the surface of the developed embryo. (13, 20, 61, 62). Our results were similar to those reported by Eberlein (20); the differences can be attributed to a slightly different heat shock protocol, different fly strains, and the use of confocal imaging instead of cuticle staining for scoring.

Defect	E-Cadherin-GFP		Moesin-GFP		Eberlein (1985)	
	N	Prevalence	N	Prevalence	N	Prevalence
Failure Germ Band Extension	49	8%	28	0%	--	--
Failure Germ Band Retraction	44	32%	29	21%	249	20%
Failure Dorsal Closure	44	43%	29	31%	--	--
Head Defect	46	61%	30	80%	249	23%
Segmentation Defect	24	17%	19	42%	249	1%
Hole in Amnioserosa	51	65%	28	14%	--	--

Table 3: Prevalence of post-heat shock developmental defects. Note that not all embryos were scorable for every defect depending on embryo orientation.

The presence of holes is positively correlated with a failure of germ band retraction, failure of dorsal closure, and head defects (Figure 27C). Note that not all embryos were scorable for every defect depending on orientation during imaging. If an

embryo was not scorable for a given defect, the embryo was not included in the prevalence or correlation calculations. Additionally, since we only imaged the embryos at two time points during post-heat shock development, the prevalence values for holes in the amnioserosa should be considered a lower limit. The positive correlation between the holes and failure of germ band retraction and dorsal closure is explainable by loss of mechanical integrity in the amnioserosa. The amnioserosa has been shown to play a critical role in the mechanical processes of germ band retraction and dorsal closure(14)(34).

5.3.3 HOLES ARE ACELLULAR

The rapid and unchecked expansion of the holes calls into question their nature. To determine the makeup of the holes, we stained E-cadherin-GFP embryos for alpha-spectrin to outline cells and with DAPI to mark nuclei. Intriguingly, holes in the amnioserosa after heat shock contain neither a nucleus nor nuclear fragments, implying that these holes are acellular voids in the tissue (Figure 27B). The embryo shown in Figure 27B was fixed at 7 hours post-heat shock, and was staged at germ band retraction. We note that the nuclei in the adjacent cells in this figure appear fragmented. Fragmentation of nuclei in the amnioserosa is a sign of apoptosis, and wide-spread apoptosis does not normally occur until the end of dorsal closure.

5.3.4 HOLES ARE NOT INITIATED BY INCREASED LEVELS OF MECHANICAL STRESS

We first considered the possible cause of hole initiation as the result of the tissue being ripped apart. This could be a result of an effective increase in mechanical stress

or a decrease in mechanical strength of the amnioserosa tissue in the dorsal to dorsolateral region. To evaluate this possibility, we used laser hole drilling to compare radial strain rates in ablated control and heat-shocked tissues. If the tissue is in fact weaker or under more stress after heat shock, we would expect the post ablation radial strain rates to be higher in heat-shocked embryos. Embryos were ablated with a single pulse from an Nd:YAG laser, and the targeted tissue was imaged once per second to determine the extent of recoil after wounding. (Figure 28A shows targets.) Using the deformation field surrounding the wound we calculated the radial strain (Figure 28B).

Because the heat shock induced holes to open on the dorsal or dorsolateral surface of the amnisoerosa, we looked to see if there were spatial differences in the mechanics of the amnioserosa by comparing recoil after ablation of the dorsolateral surface or the lateral flank in non-heat-shocked embryos during Bownes stage 12, early germ band retraction (12D and 12L in the Figure 28A and C). There appears to be no difference in the strain rates for these two locations, implying that during normal development, there is not extra stress in the dorsal-lateral portion of the tissue as compared to the lateral flank that would cause the former to be more susceptible to hole formation. We then looked to see if there was a temporal difference in the mechanics of the dorsolateral portion of the amnioserosa. We compared the strain calculated from ablations in the dorsal-lateral region of the amnioserosa in control embryos during stage 8 (germ band elongation) and stage 12 embryos (8D and 12D in the Figure 28A and C). As in the previous experiments, the strain rates were comparable. This result implies that during normal development, there is no change in stress in the dorsolateral region of the amnioserosa between these two stages.

Next, we looked at how the heat-shocked tissue compares to the non-shocked tissue. When ablation experiments were performed on the dorsolateral heat-shocked amnioserosa tissue during stage 8 (compare 8D-HS to 8D in Figure 30C), initial strain rates are similar to those of control embryos; however, the heat shocked tissue actually recovers more quickly than the non-shocked tissue. When hole drilling of the dorsolateral heat-shocked amnioserosa during stage 12 was compared to non-shocked tissue at the same stage (compare 12D-HS to 12D Figure 28C), the heat-shocked tissue recoils slightly less. This evidence shows that there is no excess mechanical stress or tissue-wide weakening of the amnioserosa that would allow adjacent cells to be pulled apart to create a hole. To the contrary, holes resulting from laser ablation in heat-shocked tissue appear less likely to expand than laser-induced holes in control tissue.

It is interesting to note that the holes that result from laser hole drilling do not respond like the holes seen as a result of heat shock. The tissue after laser hole drilling only expands slightly before coming to equilibrium, whereas the heat-shocked tissue grows steadily over a much longer timescale Figure 28B-D). This response in heat-shocked tissue points to a fundamental difference between laser-induced holes and heat-shock-induced holes. Laser ablation appears to trigger a wound-healing response

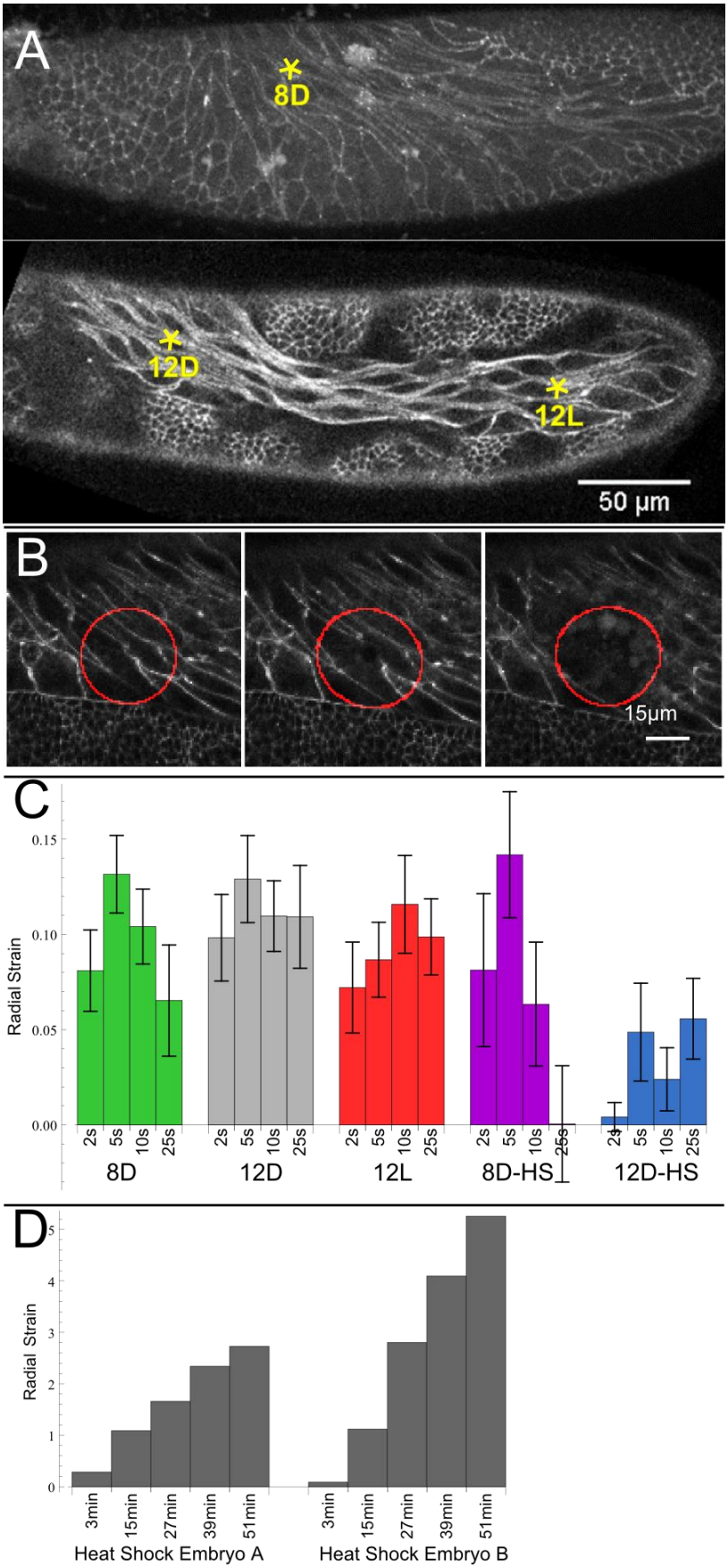

Figure 28. Mechanical stress of amnioserosa tissue after hole drilling. (**A**) Hole drilling by laser ablation targets (*) are shown for specific stages (Bownes stage: 8, germ band extension; 12, germ band retraction) and locations in the amnioserosa (D, dorsal; L, lateral). (**B**) Strain is calculated by centering a circle (16µm radius shown) on the targeted point in a pre-ablated tissue. As the tissue recoils through time, deformation of this circle is tracked with bUnwarpJ and used to calculate average radial strain (see text for details). (**C**) Radial strain versus time is plotted for laser-induced holes at various locations, stages, and heat shock treatments. (Nomenclature as in (**A**); HS, heat shock only where indicated) Error bars indicate standard error of the mean. Number of samples are as follows: 8D, n=9; 12D, n=11; 12L, n=11; 8D-HS, n=12; 12D-HS, n=8. (**D**) Radial strain versus time is plotted for heat shock-

that is not typically seen in heat-shock induced holes. Although there are examples of holes healing, this was found in only 12% (n=33, GFP-E-Cadherin) of heat-shocked embryos not exposed to continuous imaging and 17% (n=43, all strains examined in Figure 31) of continuously imaged heat-shocked embryos. In the rare cases of embryos with heat-shock induced holes that do heal, the holes did not grow to more than the width of a cell and there were no signs of later developmental defects. The lack of a wound-healing response in the large majority of heat-shock-induced holes suggests that the surrounding cells do not detect or cannot correctly respond to the presence of a hole. Since holes were not found to be the result of excess mechanical stress, we next investigated the hypothesis that they were the result of weak adhesion between cells.

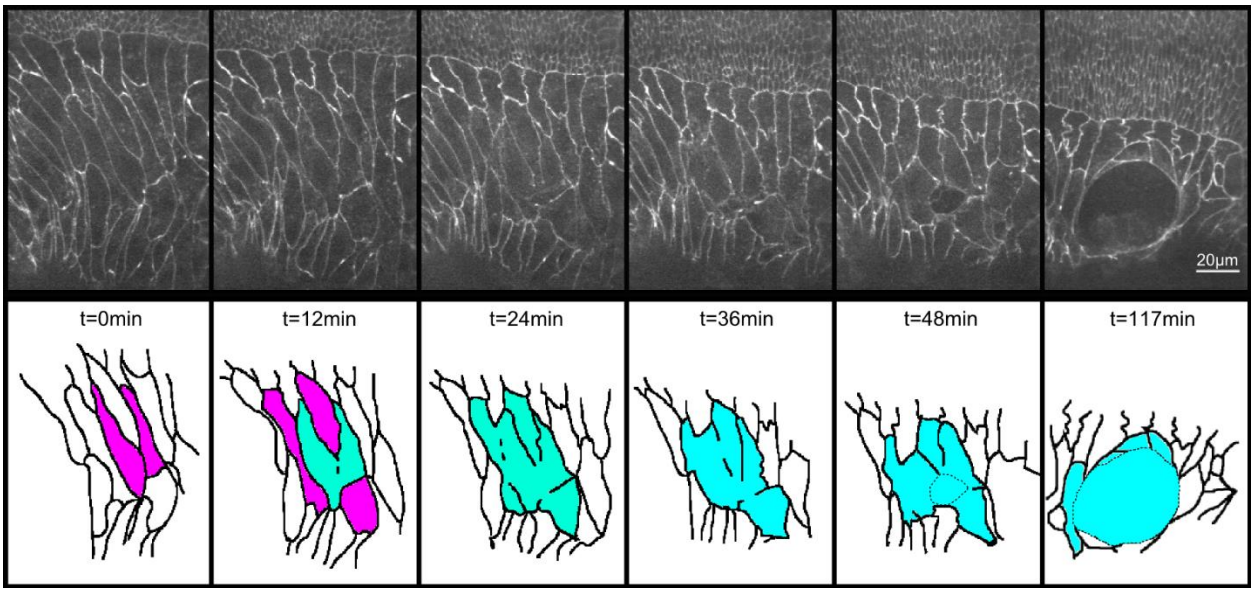

Figure 29. Cell edge failure. Timelapse images show a heat-shock induced hole opening in the amnioserosa (top). The lower panels are simplified tracings of cells in the upper images. Purple cells indicated cells that are about to become part of the hole. Blue coloring indicates cells and a cellular space which contributes to the hole. Dotted lines show hole boundary.

5.3.5 HOLES ARE NOT INITIATED DUE TO A TISSUE-WIDE REDUCTION OF ADHERENS JUNCTIONS

Figure 29 shows an example of a hole opening during germ band retraction in the amnioserosa. As seen in the timelapse images, the hole appears to open after the failure of a cell-cell boundary. This could be a result of too few or weakened adherens junctions.

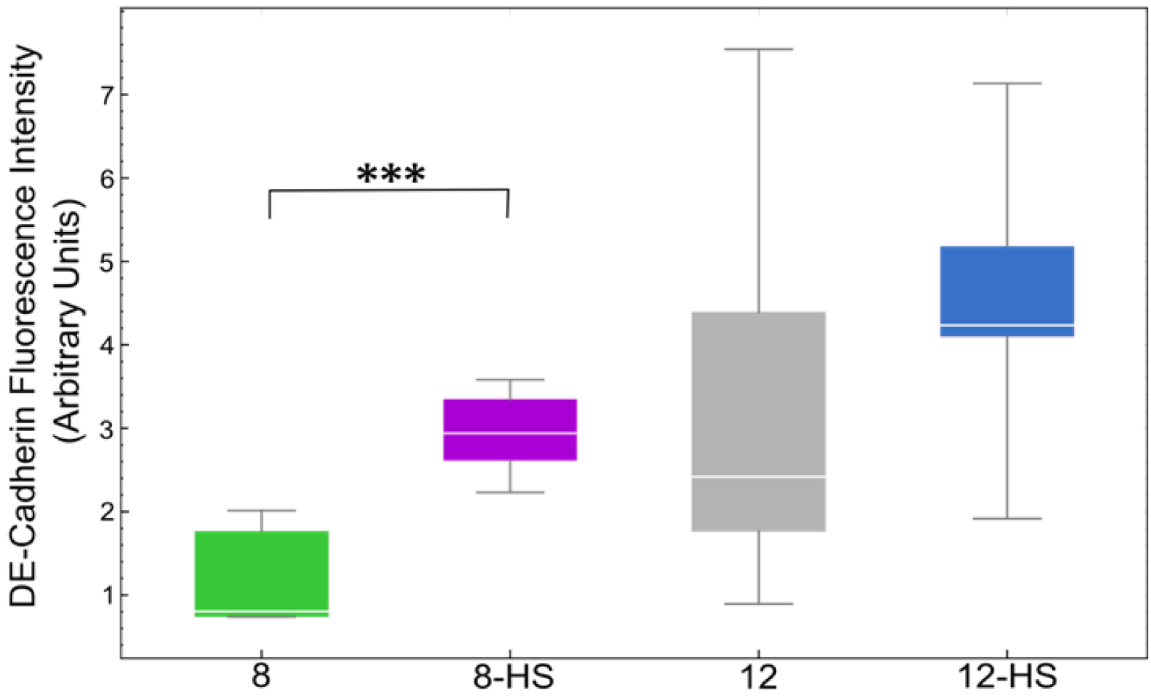

Figure 30. DE-Cadherin Expression. DE-Cadherin antibody staining localized to cell edges during germ band extension (8) and germ band retraction (12) is compared in control and heat-shocked (HS) embryos. The distributions of fluorescence intensity are plotted as box and whiskers marking the median value, inter-quartile range, and full range of the intensity distribution. *** p-value < 0.01. (8: n = 4; 8-HS: n = 7; 12: n = 8; 12-HS: n = 12).

To compare E-cadherin densities between control and heat-shocked embryos, we stained for E-cadherin during germ band extension (stage 8) and germ band retraction (stage 12) for both control and heat-shocked embryos. Figure 30 shows that embryos that were exposed to a heat shock during gastrulation actually have an increase in levels of DE-Cadherin as compared to control embryos of the same stage. In fact, the levels of cadherin found in the heat shocked embryos during germ band extension (stage 8) are more comparable to the levels of cadherin found in control embryos during stage 12, germ band retraction. This finding rejects the hypothesis that E-cadherin levels are lowered after heat shock. Considering the findings that there is no excess stress in the amnioserosa from the hole-drilling experiments and there is an increase in cadherin expression, we now consider a hypothesis that the timing of the heat-shocked tissues are misregulated.

5.3.6 DEVELOPMENTAL TIMING IS DELAYED

The timelines in Figure 31 compare the timing of heat-shocked and control embryos with identified developmental stages for each embryo. These embryos were imaged continuously starting as indicated by the first colored bar. The developmental stages of germ band elongation, the pause, and germ band retraction are assessed by the position of the tail end or telson of the germ band. We note the significant delay in morphological development of heat-shocked embryos compared to controls. Further, we show that the initiation of holes with red circles on each timeline. Holes open generally between four and nine hours after gastrulation, occurring when the embryo appears to be in germ band extension (stages 8 and 9) or germ band retraction (stages 12 and 13). Often, multiple holes occur in a single embryo with no obvious pattern to

the timing or location of subsequent hole occurrence. Intriguingly, if the initiation of the first hole in any heat-shocked embryo is compared to the developmental timing of control embryos, these initial heat-shock-induced holes appear when control embryos begin dorsal closure (stages 14 and 15), *i.e.*, when amnioserosa cells would normally begin to undergo apoptosis. Considering this observation, we investigate the evidence for a heat-shock-induced heterochronicity in the embryo resulting in a mature amnioserosa developing with a retarded germ band.

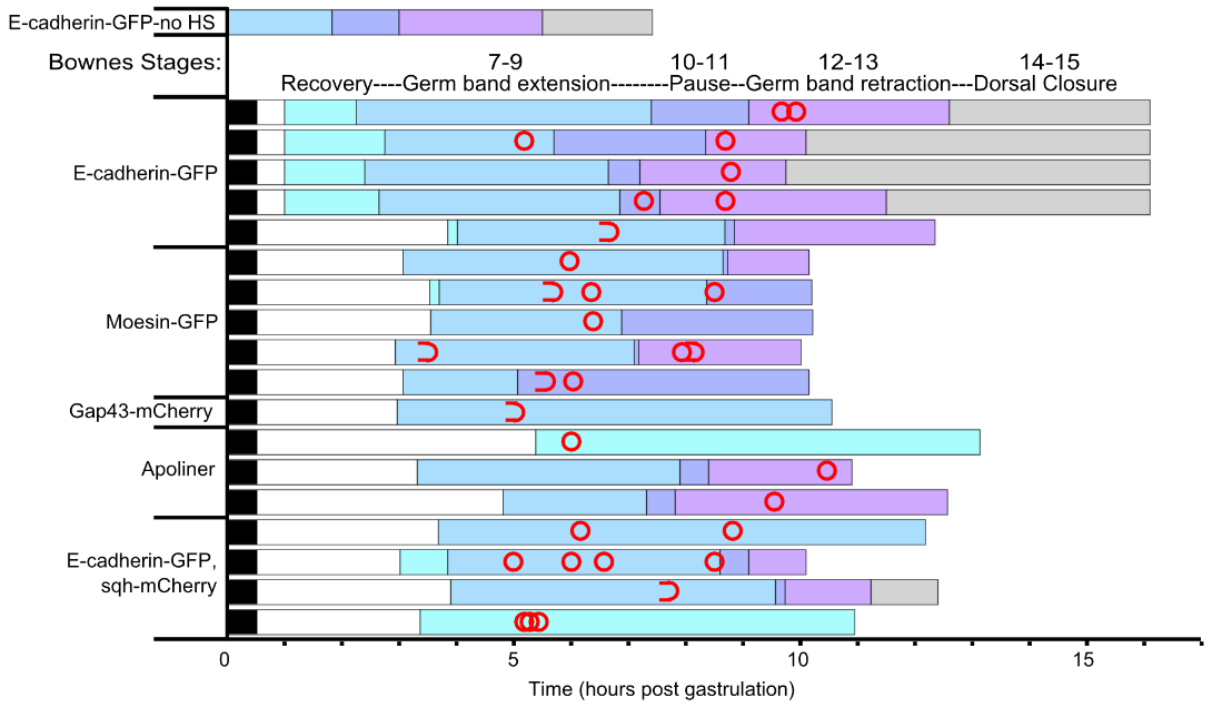

Figure 31. Timeline of developing heat-shocked embryos. Top timeline shows normal developmental progression for a control (non-heat-shocked) E-Cadherin-GFP embryo at 25°C. Remaining timelines are divided by fly strain. Bars begin at gastrulation (t=0) with a 30-min heat shock (black), followed by period of no imaging (white). The remainder of the bar indicates period of imaging. Timing of developmental stages corresponds to the legend just above the first heat-shocked E-Cadherin-GFP line. Initiation of holes is indicated (closed red circles, hole opens in view; open red circle, pre-initiated hole moves into view).

5.3.7 ABERRANT MORPHOLOGY DURING GERM BAND EXTENSION

As seen in the timeline in Figure 31 the timing of development after heat shock is greatly slowed. Starting from gastrulation, heat-shocked embryos require roughly eight hours to reach germ band retraction (stage 12) as compared to three hours in control embryos. The heat-shocked embryos also do not extend as far during germ band extension after heat shock. Figure 32A tracks the telson position through time in four different heat-shocked embryos (red) and two control embryos (black). For the control embryos, the telson position reaches a minimum of 37% of the embryo length. This marks maximum extension of the germ band. Heat-shocked embryos that fail to complete germ band retraction also fail to fully extend, as shown by the red curves that only extend to 50% of the embryo length. We also used one of the control curves to see if temperature-delayed timing would affect movement of the telson position similarly. Both black curves extend to a maximum 37% of the embryo, showing that more than just a timing delay is occurring in the heat-shocked embryos.

Failure of the germ band to fully extend corresponds to a decrease in amnioserosa cell elongation during germ band extension. We compared the rates of change of area, perimeter, and aspect ratio for amnioserosa cells during germ band extension. Amnioserosa cells in heat-shocked embryos expand their area at a rate that is barely 1/3 that of the control embryos, their perimeter expands almost 1/4 as fast, and most strikingly, their aspect ratio increases at a rate that is 1/7 as fast as cells in control embryos (Figure 32). The average aspect ratio (length divided by width of best-fit ellipse) of amnioserosa cells at maximum extension in heat-shocked embryos is 7 (152 cells from 4 embryos) compared to an aspect ratio of 8 in a control embryo with 49 cells

measured. Finally, similar to the timeline in Figure 31, we observe hole initiation (yellow points in Figure 32A) does not correlate with any specific event in germ band movement.

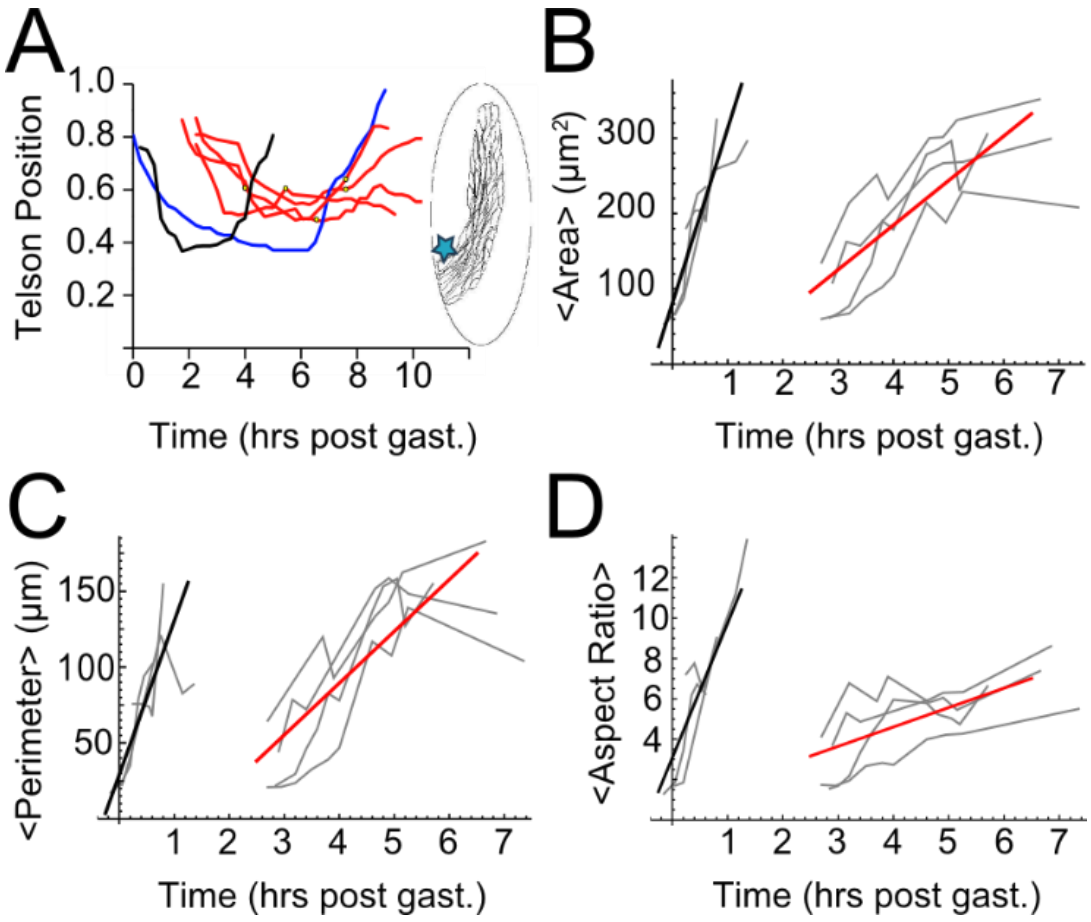

Figure 32. Cell morphology after heat shock. (A) Telson position versus time is shown starting at gastrulation and continuing through germ band retraction. The telson position is marked on the diagram of the embryo (right, blue star) as the caudal end of the germ band. In the graph (left), the telson in a control embryo (short solid black line) extends from the the posterior end (TP=1.0) towards the anterior end (TP=0.0) and reverses during germ band retraction. Four heat-shocked embryos (solid red line) are shown with holes (yellow circle) indicated at time of opening. A non-heat-shocked embryo was artificially slowed by lowering the ambient temperature during imaging to 18-19°C (long solid black line). (B-D) Morphological measuerments of amnioserosa cells were made for mean area (B), mean perimeter (C), and mean aspect ratio (D). Control (black) and heat shock (red) fits are provided to indicate differences in the rate of growth by each metric. Timing of growth initiates with germ band extension, and the separation between control and heat-shocked lines corresponds to the developmental delay (post-gastrulation) of heat-shocked embryos.

5.3.8 ACTIN ACTIVITY UPREGULATED EARLY IN HEAT-SHOCKED AMNIOSEROSA

GFP-Moesin embryos show the actin networks within cells. Although the expression is not especially strong until dorsal closure (stage 14), there appears to be an earlier difference in the cells of the heat-shocked embryos. Figure 333 shows amnioserosa cells of a heat-shocked embryo during stage 8, germ band extension. As seen in Figure 33, the actin projections in these cells are qualitatively more similar to those of cells in germ band retraction of a control embryo. This qualitative observation of increased actin activity is supported by the result of a stiffer amnioserosa tissue as detected by the hole drilling experiments. This further suggests that the amnioserosa cells are more “mature” than the rest of the embryo.

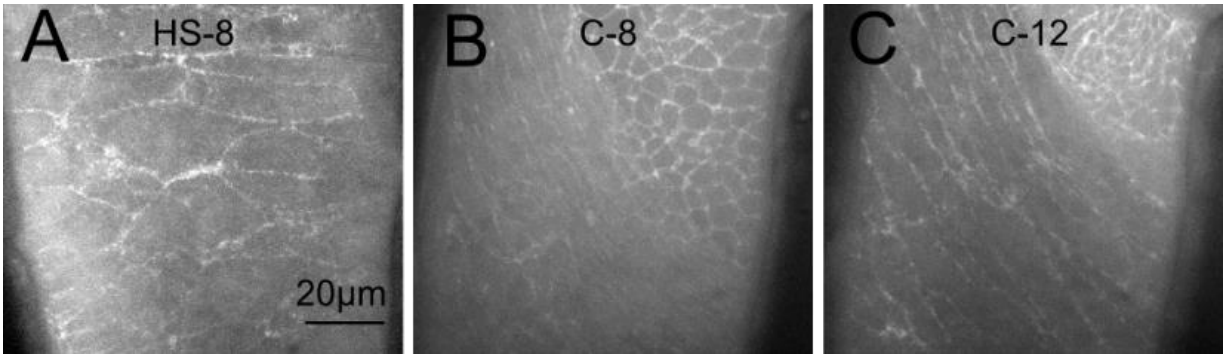

Figure 33. Actin activity. There is an increase in actin localization in amnioserosa cells in GFP-Moesin embryos between germ band extension (A) and germ band retraction (B). After heat shock, amnioserosa cells during germ band extension (C) resemble those of germ band retraction in control embryos.

5.3.9 EVIDENCE OF DELAMINATION AND APOPTOSIS

In wild-type embryos, mature amnioserosa cells entering into dorsal closure occasionally delaminate from the tissue. After extrusion, these amnioserosa cells initiate apoptosis. These delamination events help to generate force to assist in closing the lateral flanks of the germ band together (63). These delamination events typically occur in the anterior two-thirds of the amnioserosa (64). This region would correlate to the dorsal surface of the amnioserosa during extension and retraction where holes have been observed. If there is heterochronicity between tissues of the heat-shocked embryos, we would expect to see occasional amnioserosa apoptosis before the germ band enters dorsal closure.

We looked for evidence of apoptosis using live imaging of Apoliner flies, which serve as a fluorescent reporter of caspase activity (58). After heat shock, we saw no evidence of abnormal caspase activity in the amnioserosa, although this fluorescent marker is very weak at this stage. With this marker we can rule out widespread apoptosis in the amnioserosa; however, single apoptotic events may be hard to detect.

In Figure 34 we have an example of a hole opening up after an amnioserosa cell appears to be extruded from the tissue. The amnioserosa cell appears to constrict its apical surface and get pinched out of the epithelium. Immediately after this a hole opens. This is further support for the hypothesis that heat shock has induced heterochronicity in the embryo, which can result in developmental failure.

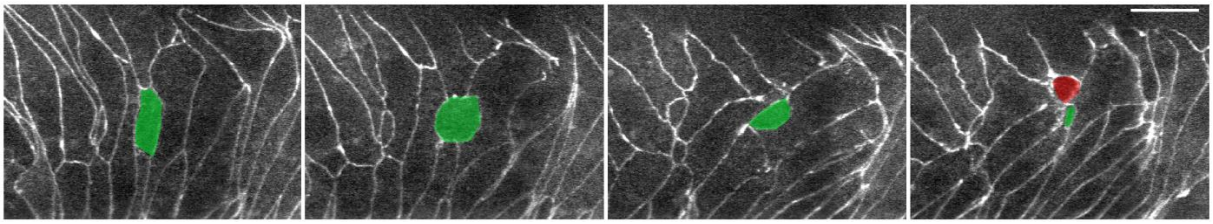

Figure 34. Cell extrusion and hole. The cell highlighted in green is being extruded from the tissue. As this cell begins to disappear from view, a hole, highlighted in red, begins to open. Scale bar is 20μm.

5.3.10 AMNIOSEROSA CELLS ELONGATE BEFORE GERM BAND EXTENDS

We also noticed that there is aberrant cell morphology following the heat shock. Immediately after heat shock, the cells in the embryo look severely disfigured (Figure 27A). Interestingly, this pattern is similar to that seen in amnioserosa cells in *arm* mutants where germ band extension fails (10). In these mutants, amnioserosa cells still rearrange their microtubules and extend, but the tissue is constricted, causing a swirling pattern of elongated cells. This could be evidence that the amnioserosa is going through cell autonomous extension before the germ band has recovered enough to begin extension. However, these cells recover from their swirled pattern before proceeding to a normal elongation process.

5.4 DISCUSSION

We have presented an *in vivo* analysis of the developmental defects known to occur in *Drosophila* embryos following a heat shock (20). The prevalence of defects match those previously reported, and we have additionally discovered the unexpected presence of holes in amnioserosa tissue. These holes are significantly correlated with specific developmental defects in germ band retraction, dorsal closure, and head

formation. Moreover, these holes are an obvious cause of disrupted mechanical integrity of the amnioserosa. We tested three possible triggers for the initiation of these holes: excess mechanical stress on amnioserosa cells; weakened adhesion between amnioserosa cells by lack of expression of E-Cadherin; or timing misregulation of heat-shocked tissues resulting in premature apoptosis of amnioserosa cells.

Our evidence shows that the holes are not a result of excessive stress on the tissue, and the failure of the amnioserosa is not a result of widespread intercellular adhesion failure. It is known that the coordinated movement of the amnioserosa and the germ band are essential for successful development (13, 14). If this coordination is altered, then development can fail. Here we have evidence that the amnioserosa cells are out of sync with the remainder of the embryo. The swirled pattern of the amnioserosa cells immediately after heat shock are consistent with *arm* mutant phenotypes in which these cells elongate prior to germ band extension (10). Furthermore, in heat-shocked embryos, the germ band does not completely extend and by measures of area, perimeter, and aspect ratio the amnioserosa cells do not fully elongate. We also have evidence of early delamination of amnioserosa cells during germ band retraction (stage 12). This finding of heterochronicity suggests that certain tissues may be more susceptible to disruption from heat shock. The amnioserosa appears to recover and then resume development at a normal pace, while the germ band lags behind. As defects caused by heat shock vary greatly based on timing of the shock, this hypersensitivity may only be transient.

A firm confirmation of this hypothesis that a heat shock causes heterochronicity between tissues will require careful experiments that show specific timing markers. This

could include looking at the temporal patterns of gene expression in the germ band and amnioserosa of heat shocked embryos. Mitochondria are also important in regards to timing of amnioserosa apoptosis. Mitochondria defragmentation is a precursor to normal delamination events in the amnioserosa during dorsal closure (64), and premature fragmentation of the mitochondria in the amnioserosa after heat shock would be an indicator of misregulated timing. It will also be essential to look at the development of the germ band on a cellular level. Does intercalation occur after heat shock as it does in normal development during germ band extension? Do the segment boundaries form appropriately and in sync with the movement of the germ band?

We also report a high prevalence of heat-shock-induced head defects, which correlate with heat-shock-induced holes in the amnioserosa. Little work has been done to understand the mechanics of the cephalic region or how the amnioserosa contributes to the development of this region, as the cephalic portion of the embryo is difficult to image by conventional techniques because of the geometry of the embryo. Head involution is one of the latest stages of embryo morphogenesis. Failure of any previous stage in development such as germ band retraction or dorsal closure may lead to the problems in head development.

The results of this paper emphasize the importance of considering developmental mechanics alongside the genetic and molecular mechanisms of development. Different tissues may have different levels of susceptibility to damage from heat shock. This inconsistent recovery within an embryo can cause a loss of coordination in the morphogenesis of interacting tissues. Such loss of coordination in

development can be caused by environmental factors and may have catastrophic effects on development.

CHAPTER 6

SUMMARY AND CONCLUSIONS

This dissertation discusses the mechanics of cells and tissues in the morphogenesis of Drosophila melanogaster embryos—namely in the amnioserosa and the germ band. These two tissues have complex interactions from germ band extension through dorsal closure. These interactions can be disrupted through a non-specific heat shock applied to the embryo during gastrulation, which can directly affect the mechanical integrity of the amnioserosa and can lead to aberrant or even failed development.

Chapter 2 sought to answer whether germ band retraction is driven by pulling of the amnioserosa or elongation of cells in the germ band using laser microsurgery and quantitative analysis of cell shape changes in the germ band. Previous ablation experiments in the germ band demonstrated that there is greatest stress anisotropy in the segments around the curve of the germ band, suggesting that the amnioserosa is pulling on the germ band in this region to help it uncurl.

Ablation of one lateral flank of the amnioserosa is sufficient to phenocopy *ush* mutants and cause a failure of germ band retraction, reiterating the mechanical importance of the amnioserosa in germ band retraction. On the other hand, even after ablation of the amnioserosa, the germ band cells still elongate, implying that cell elongation in the germ band is a cell-autonomous reshaping instead of a passive reshaping from stress applied by the amnioserosa. These results imply that cell- and

tissue-level movements during germ band retraction come from a combination of amnioserosa and germ band mechanical contributions. These results are contradicted, however, by cell shape change analysis in *ush* mutants. In these mutants, where the amnioserosa undergoes premature apoptosis and germ band retraction fails, cell elongation in the germ band does not occur. Together, all of these experiments show that there is a complex interaction between the amnioserosa and the germ band, and one tissue is not the only driving force.

Chapter 3 described a technique for separating out the active and passive mechanics in development using carbon dioxide anesthetization. This process temporarily anesthetizes embryos, but embryos are able to recover and resume development once oxygen is restored. Using this technique paired with holographic laser microsurgery, we were able to validate a low strain model for the amnioserosa during dorsal closure and show that the periodic apical area changes is the amnioserosa during dorsal closure are mechanically cell autonomous.

Chapter 3 also looks at the amnioserosa, giving measurements for the viscoelastic properties of the amnioserosa during germ band retraction using a combination of carbon dioxide anesthetization and particle tracking microrheology. These results show that the amnioserosa is a dynamic mechanical epithelium. At the beginning of retraction, when cells are extremely elongated, the viscosity is approximately 17 Poise, but then decreases to reach a value of 8 Poise by the end of retraction. There is also a slight anisotropy in the intracellular diffusion of particles, with movement being more restricted along the short axis of the cells. As the germ band

retracts and the amnioserosa cells round up, this anisotropy disappears, and the viscosity drops by half.

Chapter 4 then looks at how morphogenesis fails after an environmental perturbation—namely a non-specific heat shock. Embryos exposed to a 30 minute 38ºC heat shock at gastrulation experience developmental defects hours later during the stages of germ band retraction, dorsal closure, and head involution. These defects correlate with the presence of holes in the amnioserosa after a shock. These holes cause the amnioserosa to lose mechanical integrity, which later results in the observed defects.

The cause of these holes has been difficult to determine. These holes are not a result of reduction in E-cadherin levels or excess stress on the tissue. Instead, our results point to a possible heterochronicity between the amnioserosa and the germ band after heat shock. The amnioserosa exhibits properties and behavior that are usually seen during dorsal closure – including delamination events, increased actin localization, and lessened cell elongation – even though the germ band is still extending.

Together, all of the experiments and analysis presented in this dissertation demonstrate the complex mechanical interactions of tissues involved in morphogenesis. The amnioserosa is a dynamic tissue which plays a critical role in unfurling the germ band during germ band retraction. If the mechanical integrity of this tissue is lost, development is compromised. A simple non-specific heat shock is enough to disrupt the mechanical integrity of the amnioserosa and cause a range of developmental defects for the embryo; however, more work needs to be done to understand the

molecular mechanisms of how a heat shock leads to mechanical failure of the amnioserosa.

Our results here demonstrate the importance of understanding the mechanics of morphogenesis in order to understand how developmental defects occur, specifically those induced by environmental insult. Our heat shock study focuses on the amnioserosa; however, mechanical aberrations may not be limited to this tissue. Future experiments need to include a study of the effects of the heat shock on other tissues, especially the germ band and the cephalic region. Results from Chapter 2 indicate that the germ band contributes mechanically to germ band retraction. A careful analysis of cell-level contributions of the germ band after heat shock will tell whether there is defective development in the germ band and if this contributes to the observed defects. We also report that incomplete or failed head involution is a prevalent defect after gastrulae heat shock. Little work has been done in the field to study the mechanics of the cephalic region and head involution; however, three dimensional imaging techniques that have recently been developed will make these measurements more feasible. These experiments, paired with modeling techniques will help to discern the contributions of mechanical abnormalities in each tissue to the different developmental defects to give a complete analysis of the effects of heat shock on the mechanics of morphogenesis.

REFERENCES

1. Alberts, B., A. Johnson, J. Lewis, M. Ragg, K. Roberts, et al. 2002. Molecular Biology of the Cell (4th edn). Garland Science.

2. Kiehart, D.P. 1990. Molecular genetic dissection of myosin heavy chain function. Cell. 60: 347–350.

3. Bier, E. 2005. Drosophila, the golden bug, emerges as a tool for human genetics. Nature Reviews Genetics. 6: 9–23.

4. Hall, A. 1998. Rho GTPases and the actin cytoskeleton. Science. 279: 509.

5. Margaritis, L., F. Kafatos, and W. Petri. 1980. The eggshell of Drosophila melanogaster. I. Fine structure of the layers and regions of the wild-type eggshell. Journal of cell science. 43: 1–35.

6. Brody, T.B. 2013. The Interactive Fly.

7. Bownes, M. 1975. A photographic study of development in the living embryo of Drosophila melanogaster. Journal of Embryology and Experimental Morphology. 33: 789–801.

8. Tadros, W., and H.D. Lipshitz. 2009. The maternal-to-zygotic transition: a play in two acts. Development. 136: 3033–3042.

9. Sweeton, D., S. Parks, M. Costa, and E. Wieschaus. 1991. Gastrulation in Drosophila: the formation of the ventral furrow and posterior midgut invaginations. Development. 112: 775–789.

10. Pope, K.L., and T.J. Harris. 2008. Control of cell flattening and junctional remodeling during squamous epithelial morphogenesis in Drosophila. Development. 135: 2227–2238.

11. Irvine, K.D., and E. Wieschaus. 1994. Cell intercalation during Drosophila germband extension and its regulation by pair-rule segmentation genes. Development. 120: 827–841.

12. Schöck, F., and N. Perrimon. 2002. Cellular processes associated with germ band retraction in Drosophila. Developmental biology. 248: 29–39.

13. Frank, L.H., and C. Rushlow. 1996. A group of genes required for maintenance of the amnioserosa tissue in Drosophila. Development. 122: 1343–1352.

14. Lynch, H.E., S.M. Crews, B. Rosenthal, E. Kim, R. Gish, et al. 2013. Cellular mechanics of germ band retraction in< i> Drosophila</i>. Developmental biology. 384: 205–213.

15. Hutson, M.S., and X. Ma. 2008. Mechanical aspects of developmental biology: perspectives On Growth and Form in the (post)-genomic age. Physical Biology. 5: 015001.

16. Ritossa, F. 1962. A new puffing pattern induced by temperature shock and DNP in Drosophila. Experientia. 18: 571–573.

17. Burdon, R.H. 1986. Heat shock and the heat shock proteins. Biochemical Journal. 240: 313.

18. Lindquist, S. 1986. The heat-shock response. Annual review of biochemistry. 55: 1151–1191.

19. Kregel, K.C. 2002. Invited review: heat shock proteins: modifying factors in physiological stress responses and acquired thermotolerance. Journal of Applied Physiology. 92: 2177–2186.

20. Eberlein, S. 1986. Stage specific embryonic defects following heat shock in Drosophila. Developmental genetics. 6: 179–197.

21. Lamka, M.L., and H.D. Lipshitz. 1999. Role of the amnioserosa in germ band retraction of the Drosophila melanogaster embryo. Developmental biology. 214: 102–112.

22. Yip, M., M.L. Lamka, and H.D. Lipshitz. 1997. Control of germ-band retraction in Drosophila by the zinc-finger protein HINDSIGHT. Development. 124: 2129–2141.

23. Schöck, F., and N. Perrimon. 2002. Cellular Processes Associated with Germ Band Retraction in< i> Drosophila</i>. Developmental biology. 248: 29–39.

24. Oda, H., and S. Tsukita. 2001. Real-time imaging of cell-cell adherens junctions reveals that Drosophila mesoderm invagination begins with two phases of apical constriction of cells. Journal of cell science. 114: 493–501.

25. Kiehart, D.P., C.G. Galbraith, K.A. Edwards, W.L. Rickoll, and R.A. Montague. 2000. Multiple forces contribute to cell sheet morphogenesis for dorsal closure in Drosophila. The Journal of cell biology. 149: 471–490.

26. Ma, X., H.E. Lynch, P.C. Scully, and M.S. Hutson. 2009. Probing embryonic tissue mechanics with laser hole drilling. Physical biology. 6: 036004.

27. Hsouna, A., G. Nallamothu, N. Kose, M. Guinea, V. Dammai, et al. 2010. Drosophila von Hippel-Lindau tumor suppressor gene function in epithelial tubule morphogenesis. Molecular and cellular biology. 30: 3779–3794.

28. Means, J., and R. Hays. 2007. Mitochondrial membrane depolarization in Drosophila apoptosis. Cell Death \& Differentiation. 14: 383–385.

29. Mashburn, D.N., H.E. Lynch, X. Ma, and M.S. Hutson. 2012. Enabling user-guided segmentation and tracking of surface-labeled cells in time-lapse image sets of living tissues. Cytometry Part A. 81: 409–418.

30. Weisstein, E.W. 2013. Area Moment of Inertia, pp. From Mathworld—A Wolfram Web Resourse.

31. Jayasinghe, A.K., S.M. Crews, D.N. Mashburn, and M.S. Hutson. 2013. Apical Oscillations in Amnioserosa Cells: Basolateral Coupling and Mechanical Autonomy. Biophysical journal. 105: 255–265.

32. Kiehart, D.P., Y. Tokutake, M.S. Chang, M.S. Hutson, J. Wiemann, et al. 2006. Ultraviolet laser microbeam for dissection of Drosophila embryos. Cell Biology: A Laboratory Handbook, 3rd ed., JE Celis, ed.(Elsevier Academic, 2006). : 87–103.

33. Jayasinghe, A.K., J. Rohner, and M.S. Hutson. 2011. Holographic UV laser microsurgery. Biomedical optics express. 2: 2590.

34. Solon, J., A. Kaya-Çopur, J. Colombelli, and D. Brunner. 2009. Pulsed forces timed by a ratchet-like mechanism drive directed tissue movement during dorsal closure. Cell. 137: 1331–1342.

35. Azevedo, D., M. Antunes, S. Prag, X. Ma, U. Hacker, et al. 2011. DRhoGEF2 regulates cellular tension and cell pulsations in the amnioserosa during Drosophila dorsal closure. PloS one. 6: e23964.

36. Blanchard, G.B., S. Murugesu, R.J. Adams, A. Martinez-Arias, and N. Gorfinkiel. 2010. Cytoskeletal dynamics and supracellular organisation of cell shape fluctuations during dorsal closure. Development. 137: 2743–2752.

37. Hutson, M.S., J. Veldhuis, X. Ma, H.E. Lynch, P.G. Cranston, et al. 2009. Combining laser microsurgery and finite element modeling to assess cell-level epithelial mechanics. Biophysical journal. 97: 3075–3085.

38. Chen, H.H., and G.W. Brodland. 2000. Cell-level finite element studies of viscous cells in planar aggregates. Journal of biomechanical engineering. 122: 394–401.

39. Breuer, K.S. 2005. Microscale diagnostic techniques. Springer.

40. MacKintosh, F., and C. Schmidt. 1999. Microrheology. Current opinion in colloid \& interface science. 4: 300–307.

41. Mizuno, D., D. Head, F. MacKintosh, and C. Schmidt. 2008. Active and passive microrheology in equilibrium and nonequilibrium systems. Macromolecules. 41: 7194–7202.

42. Cicuta, P., and A.M. Donald. 2007. Microrheology: a review of the method and applications. Soft Matter. 3: 1449–1455.

43. Wirtz, D. 2009. Particle-tracking microrheology of living cells: principles and applications. Annual review of biophysics. 38: 301–326.

44. Daniels, B.R., B.C. Masi, and D. Wirtz. 2006. Probing Single-Cell Micromechanics In Vivo: The Microrheology of< i> C. elegans</i> Developing Embryos. Biophysical journal. 90: 4712–4719.

45. Mason, T., K. Ganesan, J. Van Zanten, D. Wirtz, and S. Kuo. 1997. Particle tracking microrheology of complex fluids. Physical Review Letters. 79: 3282–3285.

46. Panorchan, P., D. Wirtz, and Y. Tseng. 2004. Structure-function relationship of biological gels revealed by multiple-particle tracking and differential interference contrast microscopy: The case of human lamin networks. Physical Review E. 70: 041906.

47. Tsai, T.Y.C., Y.S. Choi, W. Ma, J.R. Pomerening, C. Tang, et al. 2008. Robust, tunable biological oscillations from interlinked positive and negative feedback loops. Science. 321: 126.

48. Jaqaman, K., D. Loerke, M. Mettlen, H. Kuwata, S. Grinstein, et al. 2008. Robust single-particle tracking in live-cell time-lapse sequences. Nature methods. 5: 695–702.

49. Metzler, R., and J. Klafter. 2000. The random walk’s guide to anomalous diffusion: a fractional dynamics approach. Physics reports. 339: 1–77.

50. Hiramoto, Y. 1969. Mechanical properties of the protoplasm of the sea urchin egg: I. Unfertilized egg. Experimental cell research. 56: 201–208.

51. Lee, J.S., C.M. Hale, P. Panorchan, S.B. Khatau, J.P. George, et al. 2007. Nuclear lamin A/C deficiency induces defects in cell mechanics, polarization, and migration. Biophysical journal. 93: 2542–2552.

52. Ornoy, A., and Z. Ergaz. 2010. Alcohol abuse in pregnant women: effects on the fetus and newborn, mode of action and maternal treatment. International journal of environmental research and public health. 7: 364–379.

53. Pai, Y.J., N. Abdullah, R. Mohammed, A. Rolo, N.D.E. Greene, et al. 2012. Epithelial fusion during neural tube morphogenesis. Birth Defects Research Part A: Clinical and Molecular Teratology.

54. Kofink, D., M.P. Boks, H.M. Timmers, and M.J. Kas. 2013. Epigenetic dynamics in psychiatric disorders: environmental programming of neurodevelopmental processes. Neuroscience \& Biobehavioral Reviews. 37: 831–845.

55. Moretti, M.E., B. Bar-Oz, S. Fried, and G. Koren. 2005. Maternal hyperthermia and the risk for neural tube defects in offspring: systematic review and meta-analysis. Epidemiology. 16: 216–219.

56. Edwards, M. 1998. Apoptosis, the heat shock response, hyperthermia, birth defects, disease and cancer. Where are the common links? Cell stress \& chaperones. 3: 213.

57. Edwards, M.J., K. Shiota, M.S. Smith, and D.A. Walsh. 1995. Hyperthermia and birth defects. Reproductive Toxicology. 9: 411–425.

58. Bardet, P.-L., G. Kolahgar, A. Mynett, I. Miguel-Aliaga, J. Briscoe, et al. 2008. A fluorescent reporter of caspase activity for live imaging. Proceedings of the National Academy of Sciences. 105: 13901–13905.

59. Sullivan, W., M. Ashburner, R.S. Hawley, and others. 2000. Drosophila protocols. Cold Spring Harbor Laboratory Press.

60. Arganda-Carreras, I., C.O. Sorzano, R. Marabini, J.M. Carazo, C. Ortiz-de-Solorzano, et al. 2006. Consistent and elastic registration of histological sections using vector-spline regularization. Springer.

61. Roote, C.E., and S. Zusman. 1995. Functions for PS integrins in tissue adhesion, migration, and shape changes during early embryonic development in Drosophila. Developmental biology. 169: 322–336.

62. Harden, N., H.Y. Loh, W. Chia, and L. Lim. 1995. A dominant inhibitory version of the small GTP-binding protein Rac disrupts cytoskeletal structures and inhibits developmental cell shape changes in Drosophila. Development. 121: 903–914.

63. Toyama, Y., X.G. Peralta, A.R. Wells, D.P. Kiehart, and G.S. Edwards. 2008. Apoptotic force and tissue dynamics during Drosophila embryogenesis. Science Signaling. 321: 1683.

64. Muliyil, S., and M. Narasimha. 2014. Mitochondrial ROS regulates cytoskeletal and mitochondrial remodeling to tune cell and tissue dynamics in a model for wound healing. Developmental cell. 28: 239–252.